USING ANHYDRITE CRYSTALS AND WHOLE ROCK ANALYSIS IN A MISSISSIPPIAN SALT DIAPIR AS A PROXY TO DETERMINE THE PRESERVATION EXTENT OF PRIMARY SEAWATER GEOCHEMICAL FEATURES THROUGH DEFORMATION PROCESSES

Nathan Glas

Submitted in Partial Fulfillment of the Requirements
For the Degree of Bachelor of Sciences, Honours
Department of Earth Sciences
Dalhousie University, Halifax, Nova Scotia
April 2016

Distribution License

DalSpace requires agreement to this non-exclusive distribution license before your item can appear on DalSpace.

NON-EXCLUSIVE DISTRIBUTION LICENSE

You (the author(s) or copyright owner) grant to Dalhousie University the non-exclusive right to reproduce and distribute your submission worldwide in any medium.

You agree that Dalhousie University may, without changing the content, reformat the submission for the purpose of preservation.

You also agree that Dalhousie University may keep more than one copy of this submission for purposes of security, back-up and preservation.

You agree that the submission is your original work, and that you have the right to grant the rights contained in this license. You also agree that your submission does not, to the best of your knowledge, infringe upon anyone's copyright.

If the submission contains material for which you do not hold copyright, you agree that you have obtained the unrestricted permission of the copyright owner to grant Dalhousie University the rights required by this license, and that such third-party owned material is clearly identified and acknowledged within the text or content of the submission.

If the submission is based upon work that has been sponsored or supported by an agency or organization other than Dalhousie University, you assert that you have fulfilled any right of review or other obligations required by such contract or agreement.

Dalhousie University will clearly identify your name(s) as the author(s) or owner(s) of the submission, and will not make any alteration to the content of the files that you have submitted.

If you have questions regarding this license please contact the repository manager at dalspace@dal.ca.

Grant the distribution license by signing and dating below.

_____ _____

Name of signatory Date

Abstract

Evaporites provide direct evidence of seawater geochemistry and seawater crystallization through preserved fluid inclusions. Fluid inclusion analysis can be used to analyze the paleoenvironment that existed during evaporite formation when considering undeformed salt deposits. However, diapirism makes interpretation more difficult, owing to recrystallization processes that occur during deformation. The Wallace No. 1 core was drilled into one such salt dome located in the Cumberland Basin in northern Nova Scotia. The drill hole penetrated through the eastern flank of a large anticline cored with evaporites; mainly halite, anhydrite, gypsum and lesser occurrences of sylvite and carnallite. This deposit is heavily deformed and preserved beds dip between 40°-60° making it difficult to determine seawater chemistry from conventional methods such as fluid inclusion studies. However, preserved mudstone beds do exist, along with clear and dark grey-banded halite layers. In addition, thin sections show primary 'snow-on-the-roof' textures, with halite crystals being capped by anhydrite, exhibiting cyclic repetition. These preserved bedforms and textures indicate that not all of the deposit was reworked during deformation. The ability to discern preserved seawater geochemical features in salt diapirs allows for paleoclimate and paleoenvironment reconstructions to be completed. In areas that may be lacking undeformed salt deposits or other easily interpretable rocks, this can be extremely useful. This is also important considering Carboniferous evaporite basins are rare and seawater compositions changed from calcite to aragonite seas during this time period, making the ability to study salt diapirs, especially of this age, important.

Through examination of the whole rock geochemistry, including trace element compositions and anhydrite crystal chemistry, conclusions were made about the environmental conditions during primary precipitation. From these, it can be deduced that the deposit formed in a restricted basin with a large volume of brine. The basin was on the order of ~100 meters deep, with evaporite precipitation outpacing subsidence, eventually leading to a shallow sabkha-like environment persisting until the basin was closed off due to glacial or tectonic changes, with deformation beginning shortly after. The brine had a relatively consistent chemistry and only minor variation occurred throughout the existence of the basin. The basin age cannot be pinpointed exactly due to deformation, but is of Viséan age (347-331 Ma).

Keywords: Windsor Group, Cumberland Basin, Viséan age, evaporite basin, salt tectonics, salt dome preservation, snow-on-the-roof texture, paleoenvironment analysis

Acknowledgements

Firstly, I would like to thank my supervisor, Richard Cox, for providing me with an interesting thesis topic to work on and assisting in my research throughout the year. I would also like to thank Mick O'Neill from the DNR Core Warehouse for retrieving and preparing the core. Furthermore, I must thank Gordon Brown from the Dalhousie Thin Section Laboratory for taking the time to produce my thin sections; Dan MacDonald at the Dalhousie University Robert M. MacKay Electron Microprobe Laboratory for teaching me how to use the electron microprobe and assisting in the manipulation and interpretation of my data; Ricardo Silva and Philip Sedore for teaching me how to use the XRF and assisting in the analysis; Darragh O'Connor for teaching me how to use CorelDRAW to create various logs and Lawrence Plug, the honours class coordinator, for his edits and expertise. Finally, Anne-Marie Ryan helped to coordinate meetings, answer questions and critique my work. The assistance of everyone above was invaluable and greatly appreciated.

Table of Contents

Table of Figures

Table of Tables

1.0 Introduction

1.1 Objective

The Wallace Sub-basin contains Windsor Group deposits composed of sandstones, siltstones, gypsum, anhydrite and a massive salt dome of Mississippian subperiod that has been deformed into a salt diapir (Boehner, 1986). The salt diapir is composed mainly of halite (NaCl), with interstitial anhydrite ($CaSO_4$), sylvite (KCl) and carnallite ($KMgCl_3 \cdot 6H_20$) along with preserved mudstone beds (Figure 1.1 & Figure 1.2) (Boehner, 1986). The Wallace-1 core was drilled through the eastern flank of the above mentioned diapir (Figure 1.3). Despite the deformation present, halite banding, alternating between clear and dark halite, and preserved mudstone beds are seen, which may indicate that complete recrystallization did not occur.

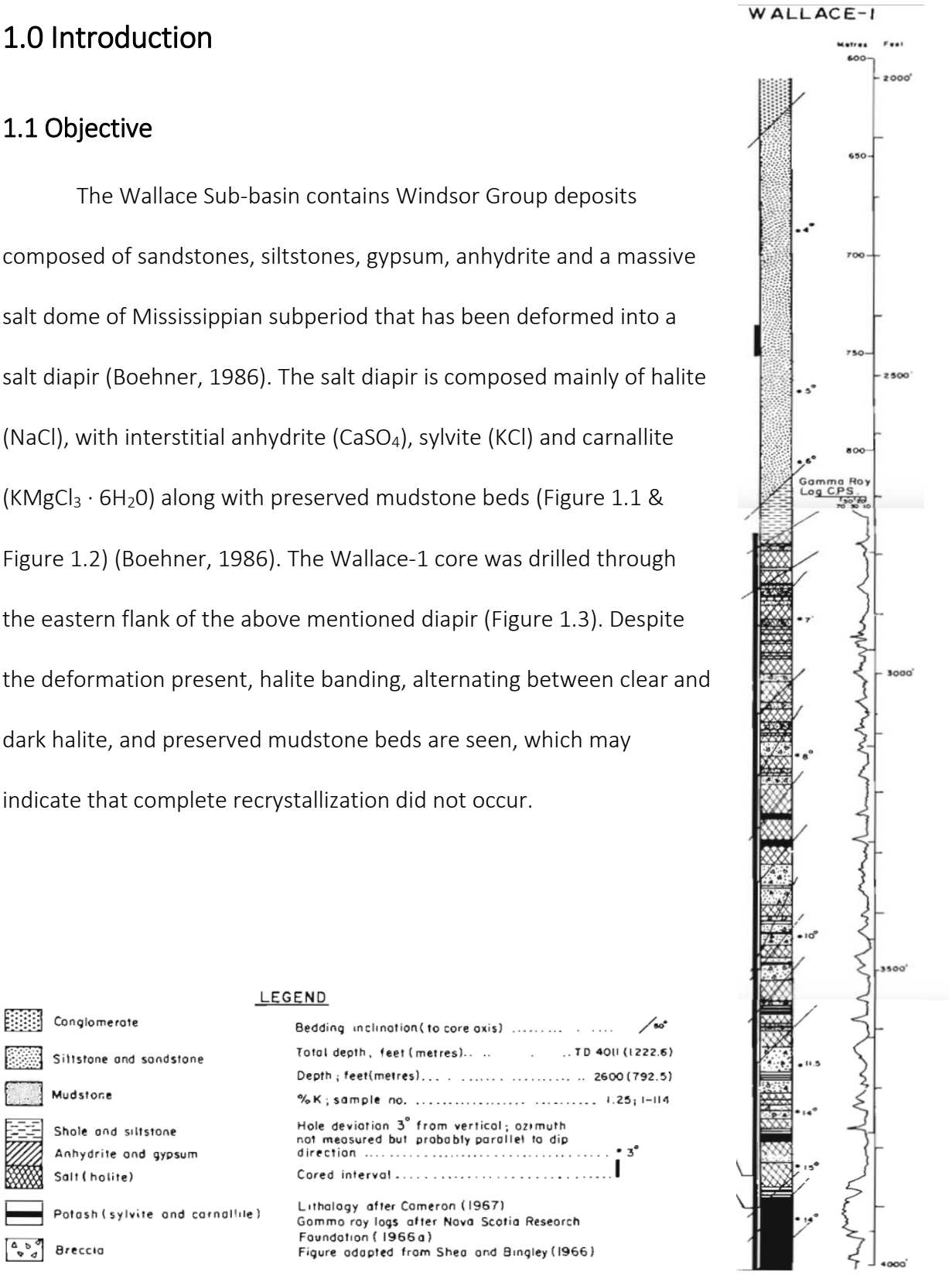

Figure 1.1: Stratigraphic log illustrating the lithologies of the Wallace-1 core (Boehner, 1986).

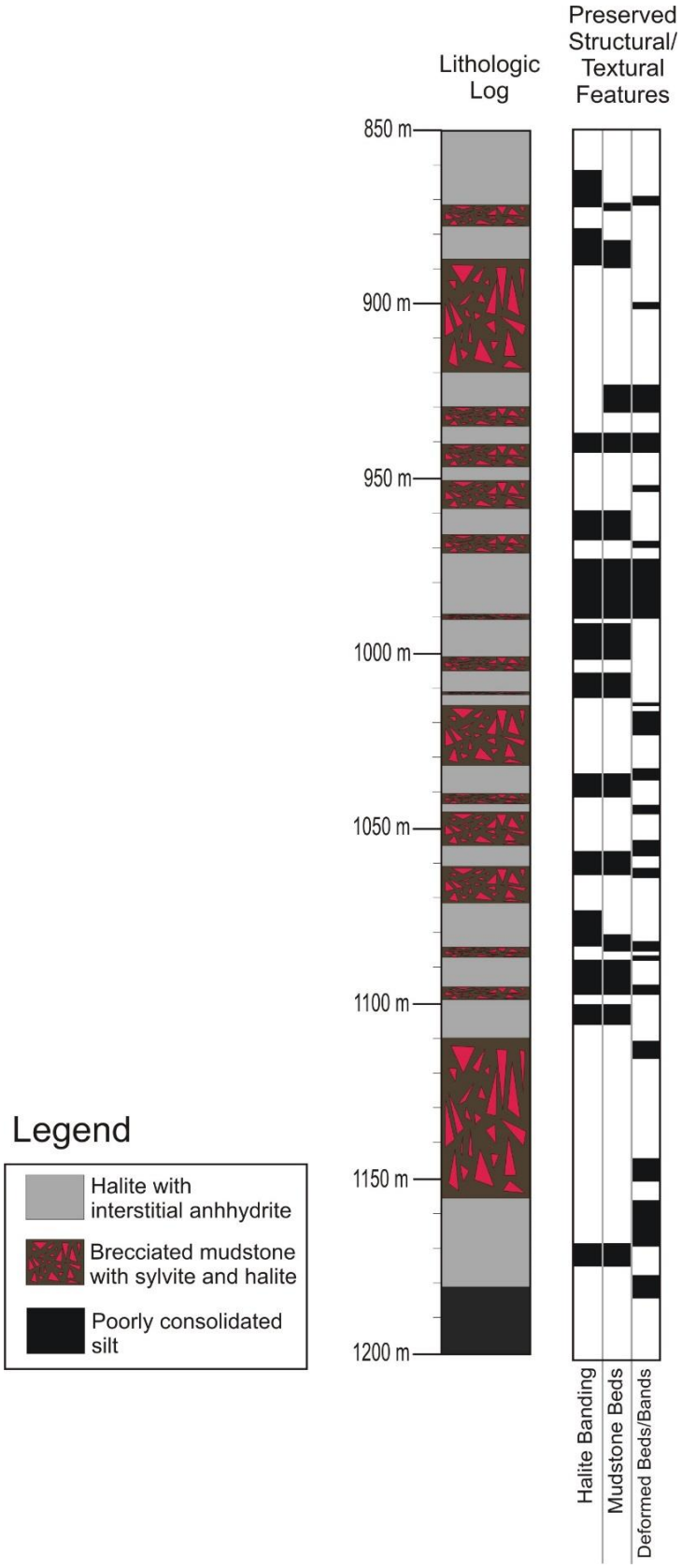

Figure 1.2: Lithologic log created to illustrate localities of preserved halite banding and preserved mudstone bedding within the Wallace-1 core.

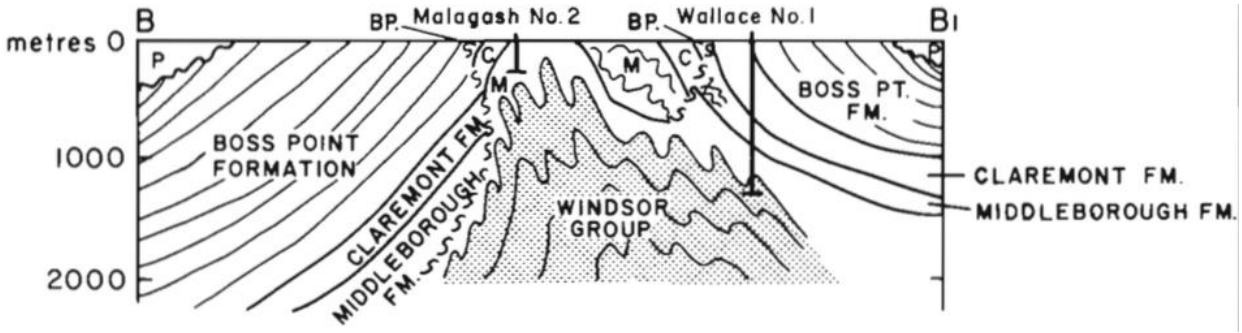

Figure 1.3: Sketch depicting location of the Wallace No. 1 drill hole and formations penetrated during drilling (Boehner, 1986).

My thesis analyzes samples collected from the above salt diapir, with the goal of determining whether any primary seawater geochemical features have been preserved, or whether deformation has completely recrystallized and reset the deposit. To ascertain this, I completed analyses using core and hand sample descriptions, petrographic descriptions, Electron Microprobe Analysis (EMPA) and X-ray Fluorescence (XRF) analysis.

All of these analyses will help constrain the oceanic environment at the time, as well as the general climate and any major climatic changes that took place over the deposition of this salt deposit. The depositional environment likely changed with time, moving from deep-water to shallow-water to a sabkha-like environment. Deep water depositional environments are comprised of gypsum and/or halite saturated bottom waters with the potential for bottom-growth crystals forming within the sediment (Warren, 1989). The surface waters have a larger degree of seawater chemistry fluctuation, allowing crystallization in surface waters, with these crystals slowly settling out (Warren, 1989). These environments also experience turbidites and mass flows which can rework sediments (Warren, 1989). Shallow water depositional environments depend greatly on the stability of the water column, but can precipitate large, bottom-growth crystals when conditions are stable (Warren, 1989). Precipitation in these basins is usually rapid and leads to the development of sabkha-like conditions (Warren, 1989). Sabkha

depositional environments are generally characterized as subaerial mud flats with ephemeral shallow water cover and commonly exist on the flanks of other systems (Warren, 1989). Sabkha deposits are commonly capped with an erosional surface (Warren, 1989).

From this, data comparisons will be made to studies completed on deposits of similar age and locality (Holt et al., 2014 & Petrychenko et al., 2002), with the intent of verifying my conclusions. The Paradox Formation of Utah and Colorado will also be used as a comparative tool due to its similar nature (Raup & Hite, 1992; Williams-Stroud, 1994).

1.2 Tests Employed

My approach is to examine bulk rock analysis and mineralogical analysis, with a focus on anhydrite crystals, to reconstruct the climate that existed during precipitation of this salt deposit. I collected, described, cut and photographed samples under plain and UV light. From this, samples were prepared and cut into double-polished wafers mounted on thin section slides.

I examined these thin sections under transmitted and reflected light microscopy to describe mineralogy, textural features and locate fluid inclusions for further study. The same sections were then used in the electron microprobe which provided mass percent data for my anhydrite crystals, giving detailed information on the major and minor elements that were incorporated into the chemical structure. This data was then used to make concentration against depth graphs to illustrate how these major and minor elements were distributed throughout the entirety of the deposit. X-ray fluorescence (XRF) analysis of hand samples aided in providing a quantitative characterization of the element distribution between these halite bands. In addition to this, samples were analyzed from the entirety of the sampled core to give an idea of the bulk geochemical changes recorded with depth. This data is helpful as a comparative tool to my

microprobe data and also to compare with the bulk geochemical data produced by Boehner (1986). Fluid inclusion analysis was originally intended to be completed but, after the petrographic studies were completed it was determined to be redundant based on the obviously altered nature of the fluid inclusions. The geochemical and trace element data was reviewed and helped to provide information about the seawater conditions during this time period and how changes in chemistry affected precipitation from seawater.

1.3 Previous Research

The rough precipitation sequence for evaporites is well known and starts with carbonates when ~50% of original seawater remains, followed by gypsum and anhydrite when ~20% of original water volume remains, then halite when ~10% of original water volume remains. Finally potassic salts, such as sylvite and carnallite, form when ~5% of the original water volume remains. Changes in temperature and density can alter the timing of evaporite precipitation, but the outline above acts as a guideline for what can be expected to precipitate as evaporation within a restricted basin continues. During sulfate mineral crystallization, gypsum generally precipitates first, with anhydrite forming as a later dehydration product. Only under specific circumstances, i.e. where water temperatures exceed ~40°C, or where the concentration of the brine is such that halite precipitation is almost possible, can primary anhydrite precipitate (Jaworska, 2012).

Numerous studies have been completed on the rocks from the Windsor Group, but none have provided adequate data on the tectonic environment, textural features and geochemical concentrations within minerals and the whole rock in the Wallace-1 core area.

Boehner (1986) as a part of the Nova Scotia Department of Mines and Energy, in conjunction with the Canada Department of Regional Economic Expansion, studied the Wallace-1 cores that were drilled and documented as a part of the report on Salt and Potash Resources in Nova Scotia (1986). Boehner (1986) provided qualitative analysis of the core (Figure 1.1) and collected geochemical data on broad sections of the core while looking for economic potash deposits, which were not found. For this reason, the study did not elaborate on the findings, or interpret the data. In addition, Boehner (1986) did not collect fine scale whole rock geochemical data, carry out detailed mineral studies, examine element concentrations within minerals or examine fluid inclusions.

A second study by Waldron et al. (2013) examined salt tectonics in the Cumberland Basin. This study did not consider preserved bedforms, look at the mineralogy of these samples, or the possible preservation of fluid inclusions despite the salt deformation that had occurred. In addition, there was little information provided about my samples due to the fact that they were collected from the edge of Waldron et al.'s (2013) study area.

Holt et al. (2014) examined fluid inclusions in halite beds of similar age to the Windsor Group in the Shubenacadie Basin, finding primary fluid inclusions and making estimates of the seawater geochemistry. Conversely, in my study, bulk rock and anhydrite crystal geochemistry provided the source of the data. The study by Holt et al. (2014) also examined samples which were diagenetically altered but not extensively deformed. This is in constrast to the deformed samples in my study, which further necessitate a different analytical strategy.

Studies of the Paradox Formation, summarized by the U.S. Geological Survey Bulletin 2000-B (Raup & Hite, 1992), found similar features to my study area. Halite dominated

successions with anhydrite laminations similar to those seen in my study were described and element concentrations showing trends that mimic those collected in my study were found (Raup & Hite, 1992). Thus, the Paradox Formation will act as a comparative tool to determine the level of preservation in my samples.

1.3.1 Modern Fluid Inclusion Analysis

The geochemical variations recorded by halite fluid inclusions are useful in determining paleo-seawater compositions. Timofeeff et al. (2001) found that halite fluid inclusions in the solar saltwork of Great Inagua Island (Bahamas) and in the supratidal sabkha of Baja California, have major ion compositions similar to modern seawater. Halite fluid inclusions from a nonmarine source in the Qaidam Basin (Western China) were found to have a distinctly different major ion composition from that of modern seawater (Timofeeff et al, 2001). The studies by Timofeeff et al. (2001) suggest that fluid inclusion analysis in modern halite samples can provide information about recent variations in seawater chemistry. By extension, the element concentrations within evaporites of Viséan age, which I use in this study, may provide a window into the major ion composition of Viséan seawater.

Timofeeff et al. (2001) also noted several possible sources of error for inferring paleo-seawater composition from fluid inclusions: i) fluid inclusions in halite may not be the direct result of seawater evaporation, but instead may be a mixture of seawater and nonmarine water that infiltrated the marine evaporite basin, incorporating evaporite salts and creating a contaminated sample, which upon re-precipitation of salt, would provide inaccurate information about the major ion composition of the seawater; and ii) as evaporation occurs, seawater composition alters, becoming more concentrated in major ions with respect to

natural seawaters. As precipitation begins to occur, element abundances vary, based on which minerals are being preferentially precipitated (Timofeeff et al., 2001). This effect illustrates the need to be able to back-calculate the original unaltered seawater geochemistry through modeling methods. This requires an understanding of the precipitation sequence, the climatic conditions at the time, and the origin of the fluids (fresh waters, seawater, etc.) that flowed into the basin.

The above issues are applicable to my research. The first issue is especially valid considering my samples were obtained from core drilled through a salt diapir, making the verification of the fluid inclusions as primary and not secondary of vital importance. This fact adds difficulty, as there is the potential for syndepositional recycling during the original precipitation event, and also the possibility of recrystallization during halokinesis, both of which would cause resetting of the fluid inclusions. After preliminary work, it was determined that fluid inclusions within my samples were unlikely to be primary and fluid inclusion analysis procedures were abandoned in favour of alternative methods.

1.3.2 Carboniferous Fluid Inclusion Analysis

Holt et al. (2014) analyzed halite samples from two localities; the Pennsylvanian Paradox Formation (Utah, USA) and the Mississippian Windsor and Mabou Groups (Shubenacadie Basin, Nova Scotia, Canada). The first sample area exhibits a similar depositional environment and shows the same preserved textures and bedforms. The second sample area provides information on samples of similar location, age, climate and source, which should provide background information relevant to my study.

Holt et al. (2014) found that calcite seas persisted throughout much of the Mississippian subperiod, transitioning to aragonite seas in the late Mississippian, with sulfur isotope values and bromide values consistent with a marine source. Major ion compositions vary considerably from modern seawater evaporation curves, likely due to the different seawater chemistry during the Carboniferous.

This difference in seawater chemistry is largely due to whether a calcite or aragonite sea is present. In the Mississippian, calcite seas existed, indicating that there was greater concentrations of Ca^{2+} in comparison to SO_4^{2-} (Holt et al., 2014). Today, aragonite seas persist, which indicates that the opposite is true. This distinction determines whether Ca^{2+} or SO_4^{2-} will be depleted first, which will control which minerals precipitate, including the mineral sequence and the amount of precipitation that occurs (Holt et al., 2014). For example, in calcite seas, SO_4^{2-} will be depleted before Ca^{2+}, making precipitation of sulfate minerals less favourable.

Petrychenko et al. (2002), studied deposits from the westernmost portion of the Maritimes Basin and found similar features. The deposit was predominantly composed of halite, with anhydrite laminations and potash-rich zones. Petrychenko et al. (2002) determined that the brine depth varied from 10-140 m and had basal halite precipitated from non-marine waters, low in Br, which transitioned to deposits formed from chloride-rich, sulfate-poor marine waters, which persisted throughout the Mississippian. Pertychenko et al. (2002) determined that the basin would have had relatively stable temperatures and seawater chemistry with slow crystallization. Fluctuations in temperature would have occurred seasonally, reaching heights of up to 60°C during summers, allowing for potash deposition (Petrychenko et al., 2002). Also present within the samples were areas of interbedded clear halite, dark halite, claystone and

anhydrite (Petrychenko et al., 2002). This study helps to provide a characterization of the depositional environment of the thick halide sequences which exist within the Maritimes Basin. This will provide a comparison for my samples, which are located in the southwestern portion of the same basin.

1.3.3 Tectonic and Stratigraphic Development

The Maritimes Basin formed at tropical latitudes during a dextral strike slip dominated tectonic environment (Waldron et al., 2013). Sub-basins are present within the Maritimes Basin, including the Cumberland basin. Waldron et al. (2013) used 16 high-resolution seismic lines, detailed outcrop descriptions and bedrock geology maps to characterize the tectonic and stratigraphic development of the basin in relation to salt tectonics (Figure 1.4).

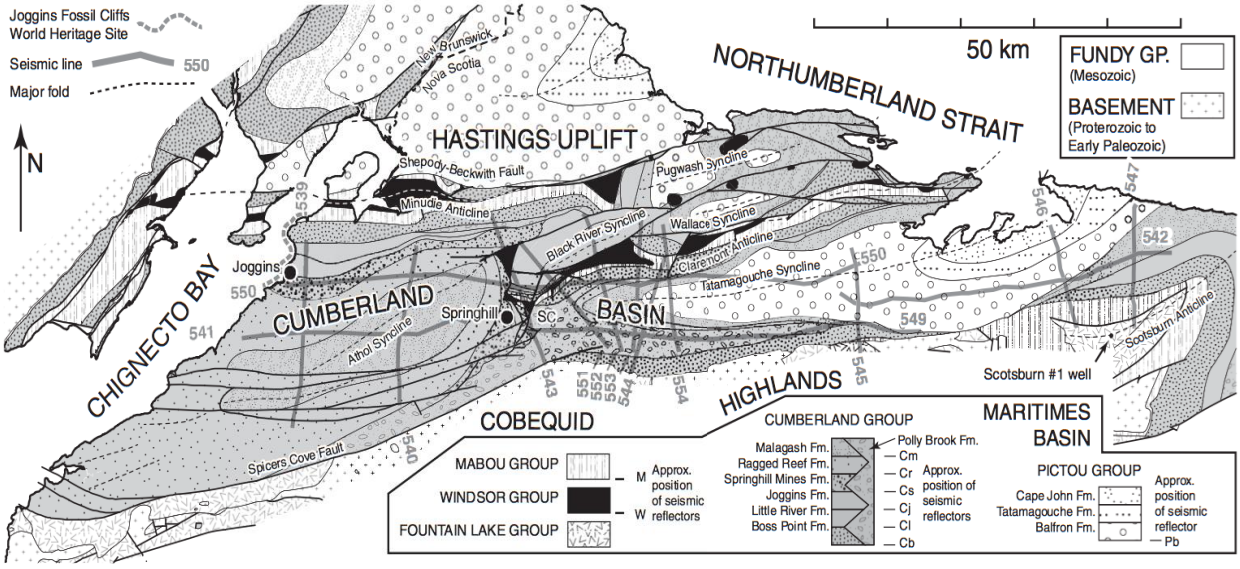

Figure 1.4: Map illustrating the Cumberland Basin, the general geology of the area, the seismic lines used in Waldron et al.'s (2013) study, along with the smaller scale synclines within the larger Cumberland Basin (Waldron et al., 2013).

The Cumberland basin shows thick Viséan aged evaporite deposits of the Windsor Group, along with overlying clastic and coal-bearing deposits (Waldron et al., 2013). Through the process of salt expulsion, large amounts of accommodation space were created (Figure 1.5),

allowing for the deposition of clastic deposits and the exceptional preservation seen at Joggins Fossil Cliffs: UNESCO World Natural Heritage Site. Waldron et al. (2013) found that this expulsion varied both in intensity and timing across the whole basin, with the western portion of the basin experiencing abundant salt expulsion during the Pennsylvanian age, while the eastern part of the basin experienced less intense salt expulsion during the earlier Mississippian subperiod (Figure 1.5).

The tectonic environment in the area facilitated vertical salt expulsion instead of horizontal expulsion, which is more common along passive continental margins (Waldron et al., 2013). Waldron et al. (2013) also found that the salt expulsion lead to the creation of broad open synclines separated by smaller and narrower isoclinal anticlines with salt diapirs at their cores (Figure 1.5).

Due to the varying forms of salt expulsion, both in time and intensity, a variety of similar, but distinct sub-basins were formed with their own specific processes and history recorded (Figure 1.5). Both symmetrical and wedge-shaped mini basins can be found (Waldron et al., 2013). The Wallace Sub-basin, the focus of my study, is within the eastern portion of the Wallace Syncline, which is in the eastern portion of the Cumberland Basin, indicating my samples would have undergone Mississippian expulsion and are likely from an isoclinal anticline with a core of salt. This suggests that these salt domes have experienced less intense halokinesis than similar salt deposits in the western portion of the basin. In turn, this indicates potential for the preservation of mineralogy, possibly including fluid inclusions and/or chemical concentration profiles within my samples.

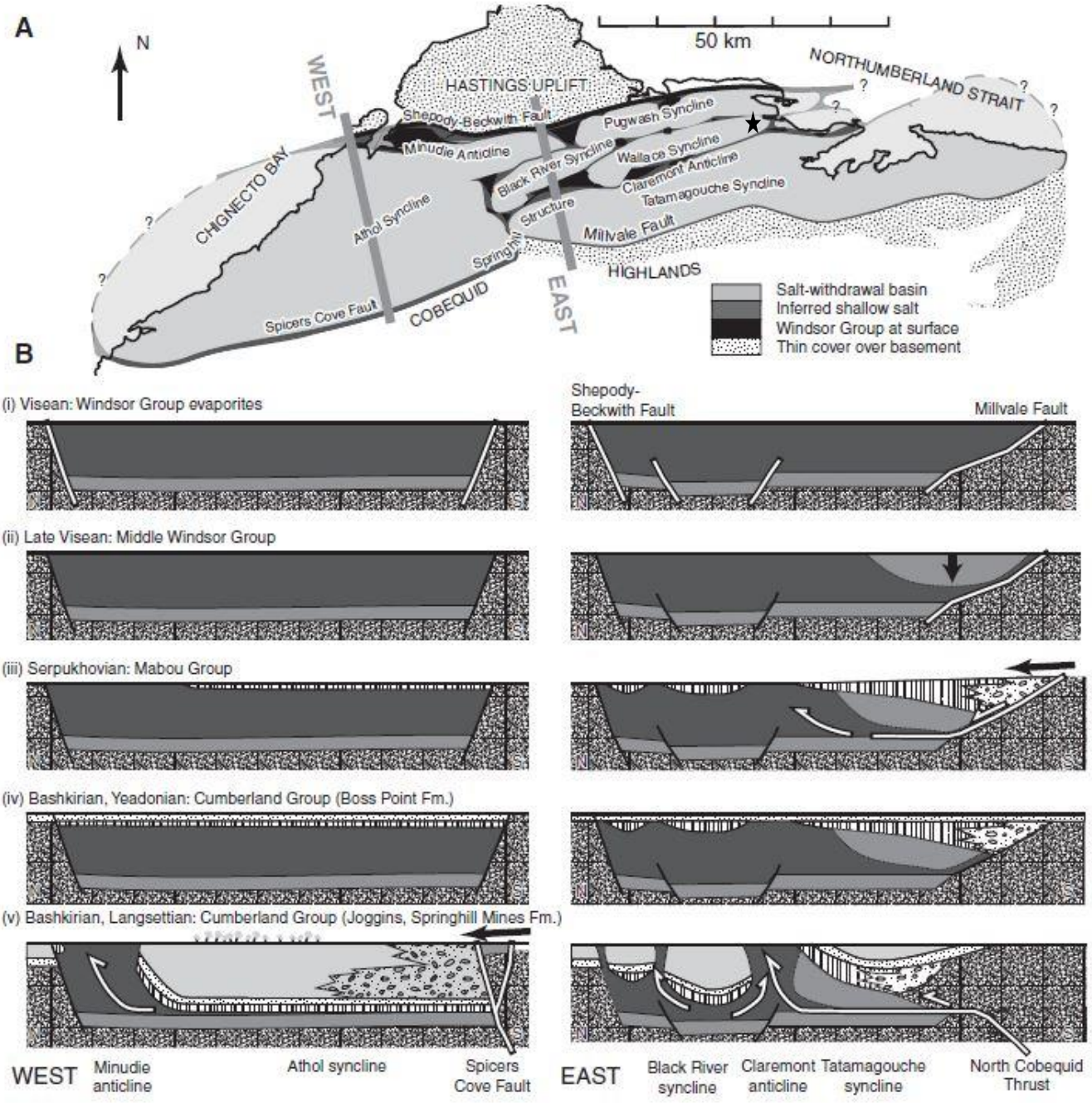

Figure 1.5: (A) Simplified map showing location of synclines within the Cumberland Basin. Map annotated with a star to indicate where the Wallace-1 core was drilled, in the eastern part of the Wallace Syncline. (B) Cross sections depicting inferred history of mini-basin development, locations shown in (A) (after Waldron et al., 2013).

2.0 Background

2.1 Regional Setting - The Windsor Group of the Cumberland Basin

2.1.1 Geologic and Paleo-climatic History

The rocks that I am studying are from the Wallace Sub-basin. The Wallace Sub-basin is within the Wallace Syncline, a part of the larger Cumberland Basin, which resides within the greater Maritimes Basin (Figure 1.5 & Figure 2.1) (Waldron et al, 2013). The Windsor Group, within the Wallace Sub-basin, contains sandstones, siltstones, gypsum, anhydrite and a salt dome (Figure 1.1) (Boehner, 1986). My study focuses on the salt dome (Figure 1.2), which is mainly halite, with interstitial anhydrite, sylvite, carnallite and preserved mudstone beds.

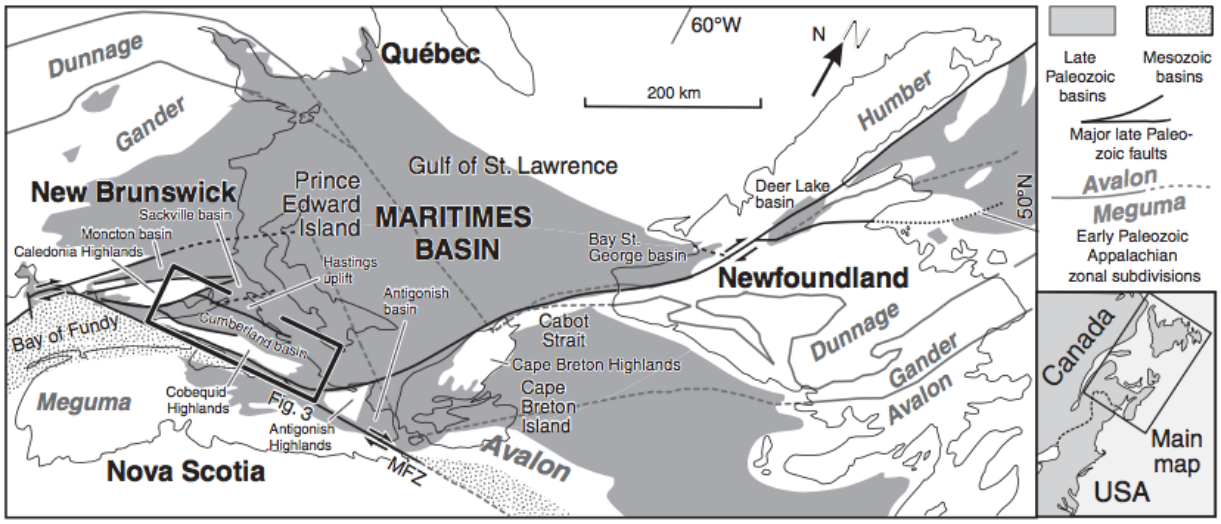

Figure 2.1: Map illustrating the extent of the Maritimes Basin, with the Cumberland Basin boxed in the bottom left (Waldron et al., 2013).

This salt deposit precipitated during the Viséan age, within the Mississippian subperiod of the Carboniferous period (Calder, 1998). During this period, Nova Scotia lay near the equator and had a semi-arid to arid climate (Figure 2.2) (Calder, 1998). Windsor Group deposits overlay the older Horton Group, with potential for a hiatus recorded during the Early- to Mid-Viséan

(Calder, 1998). This hiatus is not certain due to a lack of dateable material, but is assumed as nowhere has a continuous record been documented (Calder, 1998).

During the Mid-Viséan, the Windsor Sea infiltrated into the Maritimes rift valley and transgressed inland towards the New Brunswick Platform (Figure 2.2) (Calder, 1998). The Windsor Sea was a hypersaline tropical gulf that was restricted within the Maritimes rift valley (Schenk et al., 1994). The breach of the Maritimes rift valley by the Windsor Sea could have been due to the convergence of Gondwana and the Old Red Continent, or through regional distension across the Maritimes-Western-European province (Calder, 1998).

Evaporite deposits of several hundred meters predate rapid and repeated transgressive and regressive cycles (Boehner, 1986; Schenk et al., 1994). The transgressive cycles are more rapid and dramatic, in contrast to the lesser regressive cycles (Schenk et al., 1994). These sequences are characteristic of the upper Windsor Group and illustrate the withdrawal of the Windsor Sea from the Maritimes Rift Valley during the Late Viséan and potentially into the Early Namurian (Waldron et al., 2013; Calder, 1998). These sequences are commonly capped by halite deposits indicating maximum regression (Waldron et al., 2013). The total thickness of Windsor strata range from 800-900 m, but have been modified in areas of diapirism (Boehner, 1986).

The withdrawal of the Windsor Sea is thought to have been caused by a major phase of glaciation on Gondwana, during a marked drop in sea level, or by convergence of Euramerica, which caused thrusting, transpression and inversion during the Mid-Carboniferous (Figure 2.3) (Calder, 1998). A semi-arid to arid climate remained after the withdrawal of the Windsor Sea and into the Late Viséan (Calder, 1998).

Figure 2.2: Reconstructed map of North America showing the continental and oceanographic makeup during the Early Mississippian when the Cumberland Basin and its associated sub-basins formed and started to precipitate evaporites. Nova Scotia, illustrated by a black box on the map, was roughly 2,000 km south of the equator at this time. The map also illustrates the large Windsor Sea that infiltrated the Maritimes Rift Valley during this time (after Blakey, 2013).

Figure 2.3: Reconstructed map of North America showing the convergence of the Meguma and Avalon Terranes during the Mid-Pennsylvanian, which likely played a role both in the withdrawl of the Windsor Sea and also in the deformation of the Windsor Group evaporites. At this point, Nova Scotia, illustrated by a black box on the map, was located at the equator (after Blakey, 2013).

2.1.2 Salt Tectonic Evolution

Tectonic activity, in the form of halokinesis, which includes the mobilization and flow of subsurface salt, and the subsequent emplacement, caused mass deformation of a large portion of the Windsor Group, along with some of the Permo-Carboniferous basin-fill locally (Calder, 1998). The large kilometer-scale diapirs and salt anticlines that formed adjacent to basement fault blocks were caused by halokinesis (Calder, 1998) that may have begun as early as the Late Viséan or Early Namurian, during and after the deposition of the Mabou Group, through extensional detachment faulting of the Windsor Group on a basin-wide scale (Waldron et al., 2013; Lynch & Giles, 1995).

Namurian deformation and overthrusting has been interpreted as a consequence of the convergence of the Meguma and Avalon Terranes along the Cobequid Fault (Figure 2.3) (Waldron et al., 1989; Pe-Piper et al., 1991). The deformation of the Windsor Group and much of the Maritimes basin-fill marks a change in the structural evolution of the basin, going from extensional to transtensional and transpressive (Calder, 1998). This deformation has been linked to the Variscan and Alleghanian orogenies (Calder, 1998), with accommodation of Alleghanian thrusting in the central and southern Appalachians being created through dextral transpression (Quinlan & Beaumont, 1984). The timing of this deformation matches with that of the Mississippian-Pennsylvanian boundary, which is indicated by a widespread unconformity seen throughout the Appalachian Basin and globally.

Deformation was interrupted by a hiatus in the Mid- to Late-Namurian, followed by a change from lacustrine to fluvial depositional environment (Calder, 1998). The process of the Windsor Group evaporites migrating into diapirs and salt anticlines created massive

accommodation space through subsidence, as well as faulting (Calder, 1998). This accommodation space was then rapidly filled during the Westphalian stage (Calder, 1998). The effects of evaporite migration are illustrated by the characteristically dipping strata present at Joggins Fossils Cliffs: UNESCO World Natural Heritage Site (Calder, 1998).

2.2 Paradox Formation, Utah and Colorado

The Paradox Formation of the Hermosa Group of Pennsylvanian age in the Paradox Basin of Southeastern Utah and southwestern Colorado shows many similarities to the salt diapir of the Wallace Syncline. The Paradox Formation is composed of precipitates formed from concentrated marine brines, with little alteration afterwards (Raup & Hite, 1992). The lithology of the formation contains organic-carbon-rich carbonate shale, dolomite, anhydrite and halite, with occurences of potash (Raup & Hite, 1992). Two cores were analyzed to provide an in depth and complete study of the formation, including the lithological and the evaporite cycles that existed in this basin (Raup & Hite, 1992). The Paradox Formation contains 29 well-defined cycles composed of halite beds (Raup & Hite, 1992).

The Paradox Basin is both a structural and depositional basin, trending northwest-southeast (Raup & Hite, 1992). The basin itself is asymmetrical and covers an area of ~28,500 km^2 at present (Raup & Hite, 1992). The original thickness of the Paradox Formation was ~1500-1800 meters at greatest depth, but has been thickened locally to ~4250 meters due in part to deformation of salt bodies into diapirs (Raup & Hite, 1992). In the northeastern portion of the Paradox Basin rocks are folded, with evaporites in the cores of many of the anticlines (Raup & Hite, 1992). In anticlines further from the deformation depocenter there are halite facies that still conformably overly the underlaying sedimentary rocks (Raup & Hite, 1992). These rocks

were cored and were used for the purpose of this study to provide the least altered representation of the original environment (Raup & Hite, 1992).

The Paradox Basin subsided prior to evaporite deposition, but was quickly filled with evaporites due to the rapid precipitation of halite and other evaporites (Raup & Hite, 1992). Subsidence continued during evaporite precipitation, but was overtaken due to the speed at which precipitation occurred (Raup & Hite, 1992). The thickness of halite beds, on the order of several hundreds of feet (~100 meters), indicate that the basin must have been deep enough to allow for this much deposition before evaporite precipitation started (Raup & Hite, 1992). Given the overall thickness of the halite succession and typical subsidence rates, the first evaporites to precipitate must have done so in deeper water, which progressively shallowed as rapid evaporite deposition continued (Raup & Hite, 1992).

The cycles are dominated by halite with interbeds of anhydrite, dolomite and siliciclastic rocks, mainly organic-carbon-rich carbonate shale (Raup & Hite, 1992). The typical interbed cycle shows halite gradually transitioning into anhydrite, then silty dolomite, followed by black shale under a transgressive phase where the water level was rising, before regressing to dolomite, anhydrite and then returning to halite precipitation again (Raup & Hite, 1992). The changes in water level that caused these transgressive and regressive cycles is theorized to be a result of Gondwanaland glaciation causing changes in sea level on a global scale (Raup & Hite, 1992).

In addition to these interbeds, abundant anhydrite laminations exist within the halite beds (Raup & Hite, 1992). The halite beds are clear to cloudy and also smoky grey to light tan. The cloudy colouration is a result of brine inclusions and small anhydrite crystals (Raup & Hite,

1992). The darker tan to gray colouration can be attributed partially to organic inclusions and small fluid hydrocarbon inclusions (Raup & Hite, 1992). The halite crystals range in size from 2-5 mm on average and create layers 2-15 cm thick, with anhydrite laminations (~0.5-2 mm) between them (Raup & Hite, 1992). These anhydrite-halite occurrences often exist as alterations between clear to translucent halite and dark grey to black halite (Raup & Hite, 1992). The colouration difference is due to dispersed anhydrite crystals which diffuse the light (Raup & Hite, 1992).

Anhydrite laminations are present in dense clusters, exhibiting "snow-on-the-roof" texture (Figure 2.4) (Raup & Hite, 1992). This snow-on-the-roof texture is composed of anhydrite draping over coarse, angular, bottom-growth halite crystals (Hite, 1985). The presence of anhydrite only as draping features is interpreted to mean that the bottom-growth halite crystals were in place prior to calcium sulfate deposition (Hite, 1985). Further, it indicates that the anhydrite crystals precipitated out of the water column and settled on top of these pre-existing halite crystals (Hite, 1985). There is no evidence to determine whether these anhydrite crystals are primary or formed through dehydration of gypsum crystals after deposition (Hite, 1985). The existence of bottom growth halite and anhydrite drape features indicates that the basin depth would have been relatively shallow (Williams-Stroud, 1994).

The regular periodicity of these anhydrite laminations is explained as a result of climatic temperature changes, likely on an annual time-scale (Stewart, 1963). These temperature changes would have controlled the temperature of the brine and allowed for calcium sulfate precipitation during the warmer summer months, but not the colder winter months (Stewart,

1963). Another possibility is that seasonal storms could have caused an influx of marine or meteoric waters, rich in calcium bicarbonate that allowed for the precipitation and subsequent settling of calcium sulfate (Stewart, 1963). Both of these theories could lead to annual anhydrite laminations within a larger halite body (Stewart, 1963).

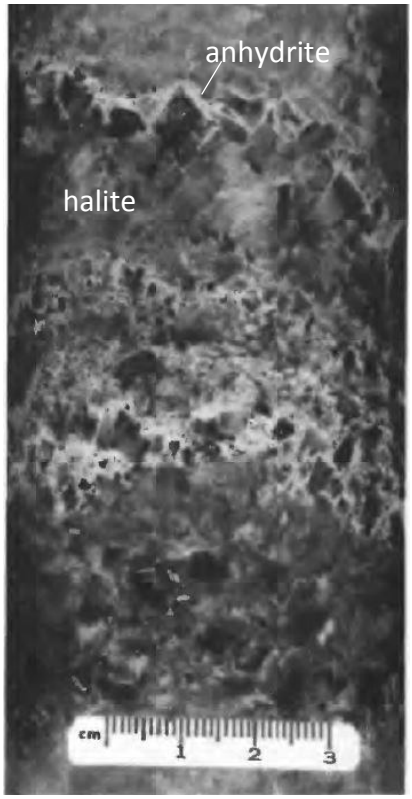

Figure 2.4: Core photograph illustrating snow-on-the-roof texture, where coarse, angular, bottom-growth halite crystals are covered by a thin layer of anhydrite crystals that precipitated out of the water column (Raup & Hite, 1992).

Raup and Hite (1992) found that the bromine concentration generally increased from the bottom to the top of the deposit (Figure 2.5). Bromine accumulates in brines and due to a small, but constant quantity of this bromine concentration being incorporated in halite through chlorine substitution, the bromine concentration within halite can be used as an indicator for the level of brine concentration, or salinity (Raup & Hite, 1992). Thus, the general increase in bromine concentration within halite indicates an increasingly concentrated brine, which was interrupted on four occasions by a significant influx of seawater, which diluted the brine and reduced salinity (Raup & Hite, 1992). The gradual, rather than rapid, increase in bromine concentration indicates that the basin must have been relatively large, and was able to accommodate a large volume of brine (Raup & Hite, 1992). However, based on morphological features such as bottom growth halite and anhydrite caps, the basin depth would not have been deep during their deposition (Williams-Stroud, 1994). The gradual and steady increase of bromine concentration also suggests constant halite precipitation throughout the life of the basin (Raup & Hite, 1992).

Sylvite is found in 19 of the 29 known evaporite cycles (Williams-Stroud, 1994). The potash mineralization mainly occurred at the top of halite sequences, in association with increased salinity and extreme brine concentration during the final stages of a particular evaporite cycle (Raup & Hite, 1992). This to low stand water levels within the basin (Raup & Hite, 1992).

Within the Paradox Basin the lack of mudcracks, ripple marks and other dessication features makes the extent of shallow-water or subaerial conditions within the basin margins unknown (Raup & Hite, 1992; Williams-Stroud, 1994).

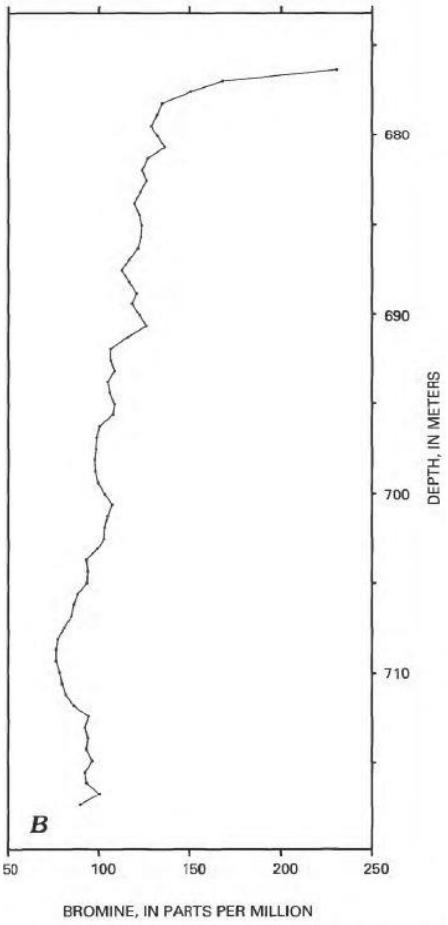

Figure 2.5: Depth profile showing the gradual increase in bromine concentration as you move from the bottom to the top of the deposit (Raup & Hite, 1992).

3.0 Methods

3.1 Core Description

The Nova Scotia Department of Natural Resources (DNR) has a core warehouse located in Stellarton, NS. During the last week of August, I described the Wallace-1 cores stored within the facility in a lab on site. The description process was completed over 4 days and involved examining ~340 meters of core, from ~850-1190 meter depth. The core was arranged in order from shallowest to deepest depth, with 1.5 meter intervals stored in each core box. Each core box contained two rows with 0.75 meters of core in each row. The core was examined and lithology, grain shape and size, colour, fractures, alteration features and stratification were

described (see Appendix A). From this, a general stratigraphic log was created to summarize my findings (Figure 1.2). Also present at the DNR core facility was the original documented description of the core completed during drilling in 1966, as well as the original description by Boehner (1986), along with a sample stratigraphic log (Figure 1.1) and geochemical data, which were used to supplement my findings.

3.2 Core Sampling

After the core had been described, my supervisor, Richard Cox, and I went through the core and marked sections of interest. These sections often related to areas that showed preserved bedding or banding, likely indicating that deformation in this region of the diapir had caused less destruction of the original structure, thus indicating the retention of the original geochemical signature. Several samples were also taken from brecciated and clearly recrystallized sections in hopes of using these samples as a comparison tool when identifying the primary nature of the anhydrite grains. In total, 42 samples were collected along the length of the core. These samples were tagged and photographed before being brought back to Dalhousie University for further evaluation. Most samples collected were half cores, though some samples

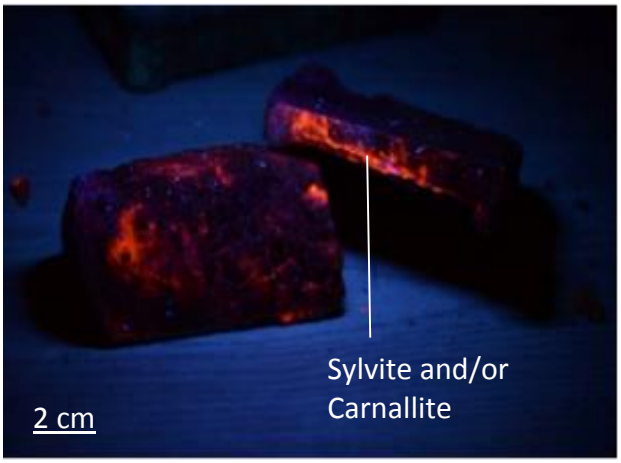

Figure 3.1: Core sample 34 from 890 meters depth photographed under a UV lamp to illuminate areas of potential sylvite or carnallite concentration, as depicted on photo.

Figure 3.2: Core sample 38 from 913 meters depth, photographed under a UV lamp to illuminate areas of potential sylvite and carnallite concentration, as depicted on photo.

taken were quarter cores. These samples were then cut using a wood saw, without water lubrication, to provide a fresh surface that could be studied in greater detail.

These fresh surfaces were subsequently described, using the same descriptors as in the overall core description (see Appendix B). The fresh faces were also photographed under plain and UV light (Figure 3.1 & Figure 3.2). The plain light photos better illustrated any preserved bedding or banding features, as well as providing high quality images of the samples for later referral. The UV light photos helped to show areas where concentrations of specific minerals were located. Areas of concentrated sylvite and carnallite gave off a red fluorescence under UV light, areas of carbonate gave off a pale green fluorescence and areas with interstitial anhydrite or fluid inclusion clusters fluoresced bright blue.

3.3 Thin Sections/Double-Polished Wafers

From the above samples, I chose 20 to be made into double-polished wafers, which were 200 microns thick and mounted on thin section slides using an acetone-based glue (Figure 3.3). Double-polished wafers were chosen as they could be described using transmitted and reflected light microscopy, analyzed in the electron microprobe and also used for fluid inclusion analysis. The thin sections were made by Gordon Brown in the Thin Sections Laboratory at Dalhousie University. The thin sections were comprised of mainly clean samples that were thought to be largely unaltered, with 3 sections being made from brecciated material to act as proxies for altered samples.

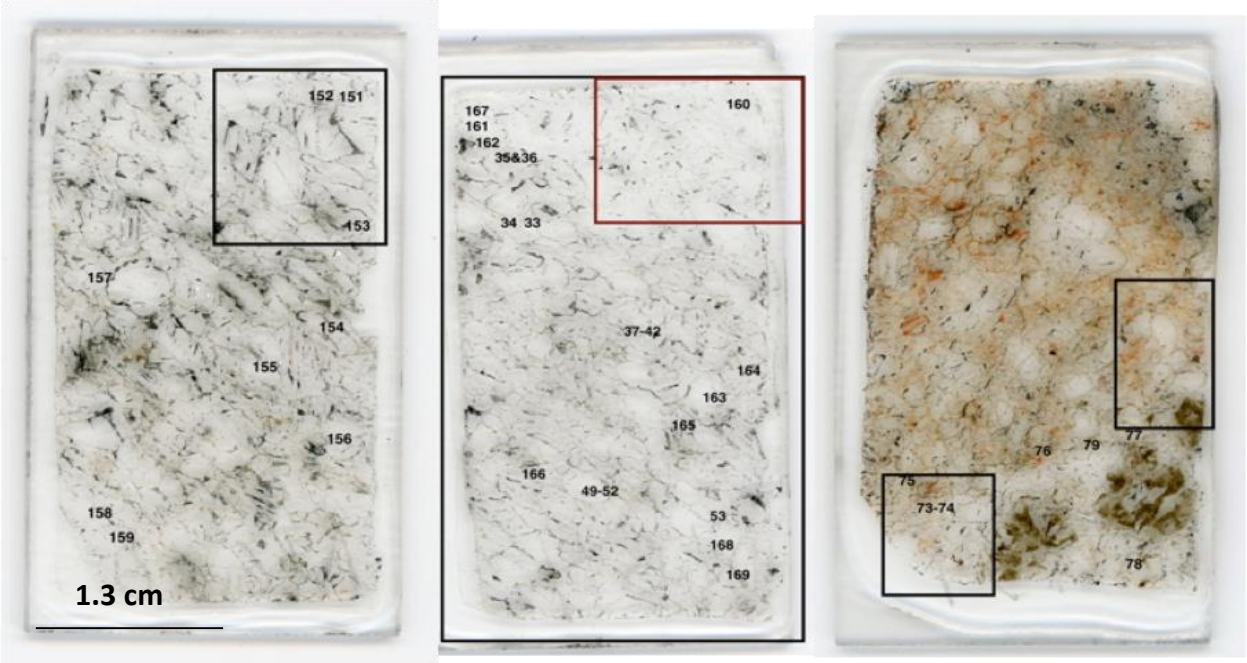

Figure 3.3: Thin section scans illustrating (from left to right) dark halite, clear halite and sylvite dominated samples. Photos annotated to show EMPA analysis points to illustrate anhydrite locations and sampling density.

3.4 X-ray Fluorescence (XRF) Analysis

Due to the coarse crystalline nature of the Wallace-1 halite, all areas needed for sampling had to be broken off and ground into a fine powder using a pestle and mortar (Figure 3.4). This helped to reduce error related to x-rays being scattered or diffracted off of the sample surface.

Figure 3.4: Photograph of powdered samples showing (from left to right) clear halite, sylvite rich and dark halite samples before being contained in vessels.

Figure 3.5: Suite of samples in examination vessels after being crushed to a powder, showing different coloured powders based on their variable compositions.

Before crushing, the pestle, mortar and scoopula were washed with alcohol and dried using kim wipes. Samples were brushed and cleaned to remove dirt or residue. Afterwards, pieces were broken off of the samples using a rock hammer or chisel and placed in the clean mortar and ground into a fine uniform powder with the pestle. The scoopula was then used to transfer the powder into small 2x3 inch plastic bags to ensure no sample contamination (Figure 3.4). The area and utensils were then cleaned and the next sample was ground.

After all samples had been ground, they were transferred into sample containers (Figure 3.5). These sample containers were made up of a sample tube, with polypropylene plastic film on either end that was clamped down by plastic rings. Polypropylene plastic film was placed on one end of the sample tube, and then secured by placing a ring over top and pressing it downwards. The powdered sample was then transferred into the sample tube, before placing and securing the top plastic film and ring over top, sealing the sample and protecting it from any contamination. The sample containers were all labeled and analyzed using a handheld XRF that had been converted for desktop use (Figure 3.6).

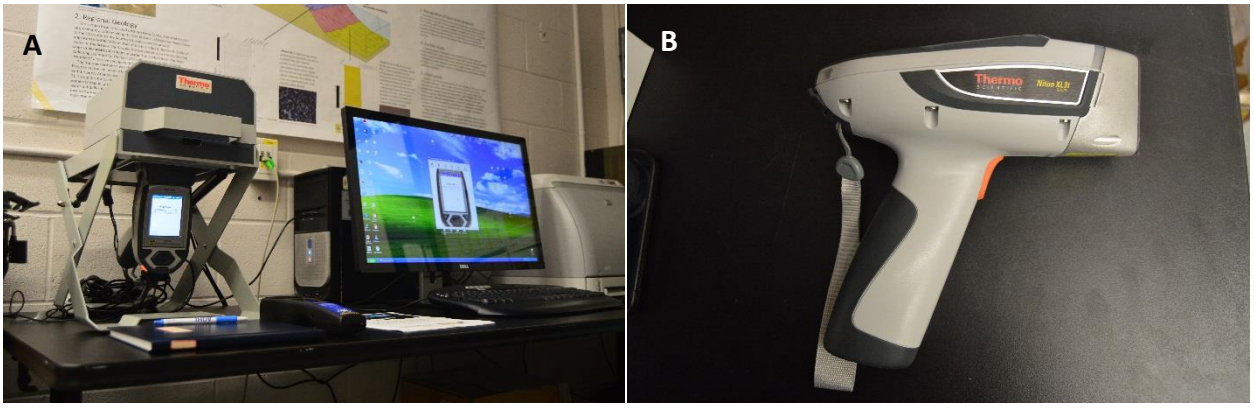

Figure 3.6: (A) XRF gun in desktop configuration with lead lined sample containment chamber. (B) Close up view of the handheld XRF gun used to complete XRF analysis.

Samples were placed in a lead lined chamber and the XRF gun was secured to the chamber, with the detection window occupying a small hole in the bottom of the chamber (Figure 3.7). The samples were then bombarded with x-rays for 180 seconds and analyzed for a suite of elements, Br, Si, S, Cl, K, Ca, Sr, Al and Fe, similar to those studied using the microprobe. Na could not be analyzed due to its low atomic mass, but was inferred through Cl concentration. Ba and Mg were not measured, but were calculated and normalized using Cl and Ca. Every fifth sample was run twice to provide a constraint on how accurate the results were and a standard was run at the beginning to calibrate the machine. A total of 27 samples were run to provide an overall bulk chemical analysis of the core, but also to provide information about the finer scale banding of clear and dark halite, with the intent of discerning the chemical differences in crystals that caused these bands to form.

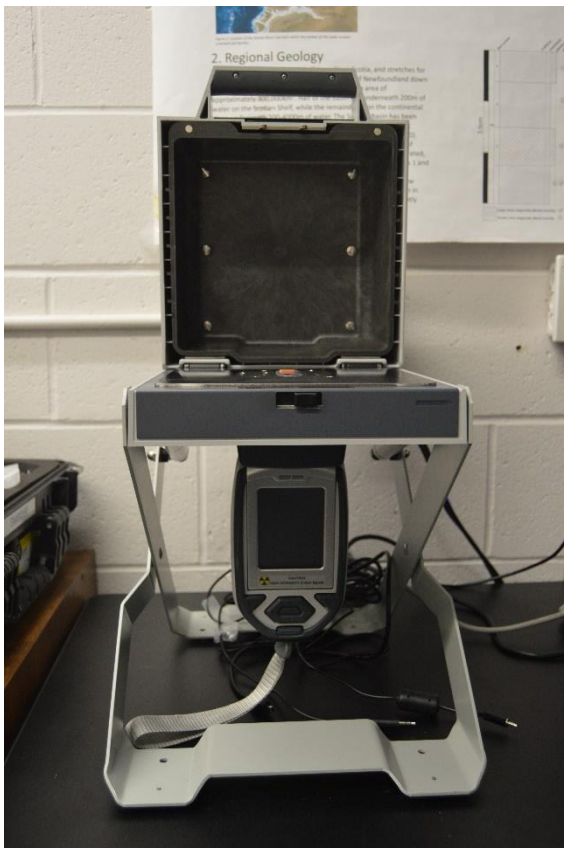

Figure 3.7: XRF gun in desktop configuration with lead lined sample containment chamber open. Samples were placed in the center of the chamber over the XRF detection window.

The XRF works by bombarding the sample with x-rays to excite electrons within the sample and cause them to give off energy in the form of x-ray waves. These x-rays pass through a beryllium detection window located on the XRF gun, where they are sorted based on wavelength to determine which element produced them. The number of x-rays detected from each element directly relates to the concentration of that element within the sample. Due to

the different energies given off by electrons falling from different orbitals, there can be peak overlaps that make it difficult to discern which element is creating the peak. The XRF uses an algorithm to help constrain which element is more likely based on the other x-rays captured and the height of the peak in question.

3.5 Electron Microprobe Analysis (EMPA)

The microprobe was used to analyze areas within the thin sections that were of interest. The microprobe provided information about the element concentrations within anhydrite crystals that I deemed primary. The formula for anhydrite is $CaSO_4$, with common substitutions being Ba, Mg and Sr, which were analyzed using the microprobe to indicate paleoenvironmental changes. The full suite of elements analyzed were Ca, S, Na, Cl, Ba, Mg, Sr, K, P and Br. Several halite samples were also analyzed for reference.

Figure 3.8: (A) Image showing the profile view of the JEOL 8200. (B) Image showing the computer screen array that displayed the camera image and the EMP analyses. (C) Second image showing the different compartments and chambers present on the JEOL 8200.

Analysis was completed at the Robert M. MacKay Electron Microprobe Laboratory in the Department of Earth Sciences at Dalhousie University. The lab is home to a JEOL 8200 superprobe (Figure 3.8) which provides quantitative analyses and images of solid or thin film samples with a spatial resolution as small as 1-2 microns. Sample preparation involves carbon coating all thin sections. The microprobe works by shooting electrons towards a vacuum sealed stage containing the thin sections of interest; the electrons have a potential energy of 15 kV. The microprobe registers primary electrons, but also measures secondary electrons that are removed from electron shells of elements in the thin section through secondary electron imaging (SEI). Within the microprobe there is a secondary electron detector that is positively charged to attract any secondary electrons present. The primary electrons are measured using wavelength dispersive spectroscopy (WDS), where wavelengths emitted pass through a beryllium detection window and are measured by crystals with different D-spacings. The JEOL 8200 superprobe at Dalhousie University contains 7 different crystals; the PETJ, PETH, LIF, LIFH, TAP, TAPH and LDE1,2. WDS has a resolution of 5 eV, which is 20 times better than the resolution of energy dispersive spectroscopy (EDS), which is also available for quick characterization of minerals and has a resolution of 128 eV.

Another feature of the microprobe that was utilized in my study was the ability to create backscattered electron (BSE) images. These are created through electron interaction with a passive detector, which scans slowly (lower beam current of ~10 kV) and registers only electrons that bounce directly to it (the detector is not positively charged to attract electrons). The detector works through measuring atomic numbers and makes a compositional map, however, it can be fooled by structural features present in the thin section.

Over two separate days, 17 samples were examined, taking roughly 200 analysis points and creating roughly 50 BSE images. This data set was given in oxide wt. %, calculating for one oxygen. This was converted to element wt. % by applying a conversion factor to remove the oxygen component. They were then converted to ppm. The data set was then averaged based on thin section, which also corresponds to depth within the core. These data were then plotted on concentration against depth graphs to illustrate the partitioning of elements with depth within the diapir.

4.0 Sample Description

4.1 Core Description

The section of core that was studied runs from ~850-1190 meter depth. The core is mainly composed of halite with areas of sylvite and carnallite, along with preserved mudstone beds and brecciated areas. No anhydrite crystals were seen in hand samples, these were only revealed using microscopy. Geochemical analysis (XRF) was used in part to help determine whether sylvite, carnallite or both were present within the core.

The halite alternates between relatively well banded clear and dark halite layers (Figure 4.1), to interlayed clear and dark halite, which makes the halite appear a light gray colour. In addition, there are areas of pink halite and areas of clear halite and dark halite without banding. The pink halite is relatively localized and only a small portion of the entire core.

Within the halite there are also areas of preserved mudstone beds (Figure 4.1). The mudstone beds range from heavily deformed mudstone clasts, too well preserved linear

dipping beds. These mudstone beds within the Wallace-1 core are often well preserved in the center of the core once split, but show obvious pitting and weathering on the external surface.

Areas of brecciation are also abundant throughout the core (Figure 4.1), with sylvite and carnallite being concentrated in these brecciated zones. This could be due to varying rheological strengths that cause brittle deformation in sylvite and carnallite layers, instead of ductile deformation as in halite. Conversely, these brecciated zones could have provided a pathway for sylvite and carnallite to be dissolved, mobilized and re-precipitated.

The preserved cycles repeat with halite gradually changing into brecciated areas dominated by sylvite and carnallite, before returning to halite dominated sequences. Towards the deeper parts of the core, the core becomes more silt and mud dominated, turning to piles of silt below 1190 meters.

Petrychenko et al. (2002) found similar features preserved in the western portion of the Maritimes Basin, including clear and dark banded halite, preserved claystone beds and sylvite-rich areas.

4.2 Hand Sample Description

The hand samples were taken as half cores and showed similar structures to that of the core. The majority were chosen due to their relationship to preserved bedding or banding and potential primary nature (Figure 4.2). Several deformed samples were also chosen as comparison tools (Figure 4.2).

The less deformed samples generally showed clear halite, with some instances of dark halite and three samples showing potentially unaltered sylvite or carnallite in the matrix. The crystals within these samples were generally coarse grained (~3-6 mm across) and well formed.

The crystals were interlocking and many had a dog-tooth shape, indicating upward growth direction and matching the snow-on-the-roof texture seen in thin section. Similar chevron style halite crystals were observed by Petrychenko et al. (2002). Conversely, some samples showed elongated crystals, likely indicating recrystallization under a preferred orientation due to stress or fluid flow.

The beds preserved were on the order of 1 cm thick and linear. The beds had varying dips, but averaged between 40-60 degrees. In some samples the mudstone did not affect the halite on either side, however, some of the mudstone beds had darker halite on either side that gradually returned to clear halite over a 1-2 cm interval, potentially indicating mud staining or that the change from halite to mud- and clay-rich deposition was gradual.

Where present, the banding seemed to show a gradual transition from clear to dark, with a ~ 1-2 cm window over which light grey halite that was composed of clear and dark halite crystals existed. Compositional changes that occurred to cause these differences in colour would have been gradual, not sudden, potentially indicating either element concentrations changed, mud content in the system increased or sea level changed.

The deformed samples collected ranged from sylvite and/or carnallite dominated to mud dominated. Some of the samples showed mud clasts within a matrix composed of sylvite and/or carnallite. Other samples showed massive mudstone with small nodules of sylvite and/or carnallite within the matrix.

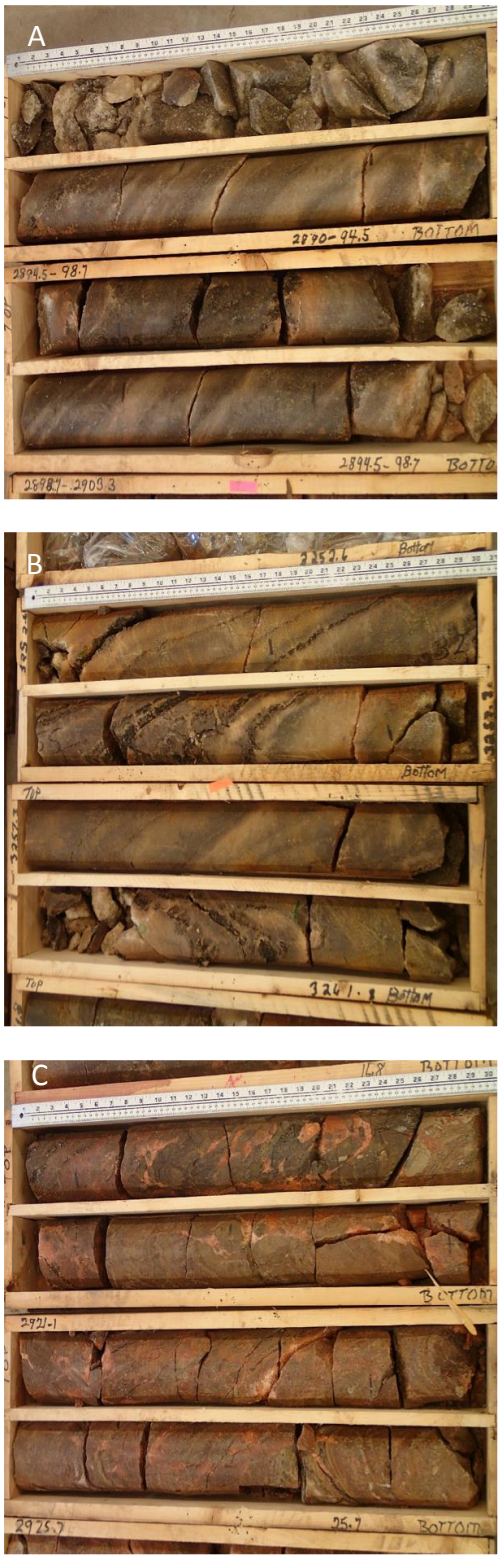

Figure 4.1: Core photographs illustrating; (A) preserved halite banding, alternating between clear and dark halite. The bands dip between 30 and 50 degrees; (B) preserved mudstone beds in a halite dominated succession. Mudstone beds dip between 40 and 60 degrees; (C) brecciated areas within a mudstone dominated succession. Sylvite and carnallite are the dominant precipitate within these brecciated areas as seen by the red-pink coloured mineral that fills the fractures. Four rows, each 0.75 meters long, are shown for each photo.

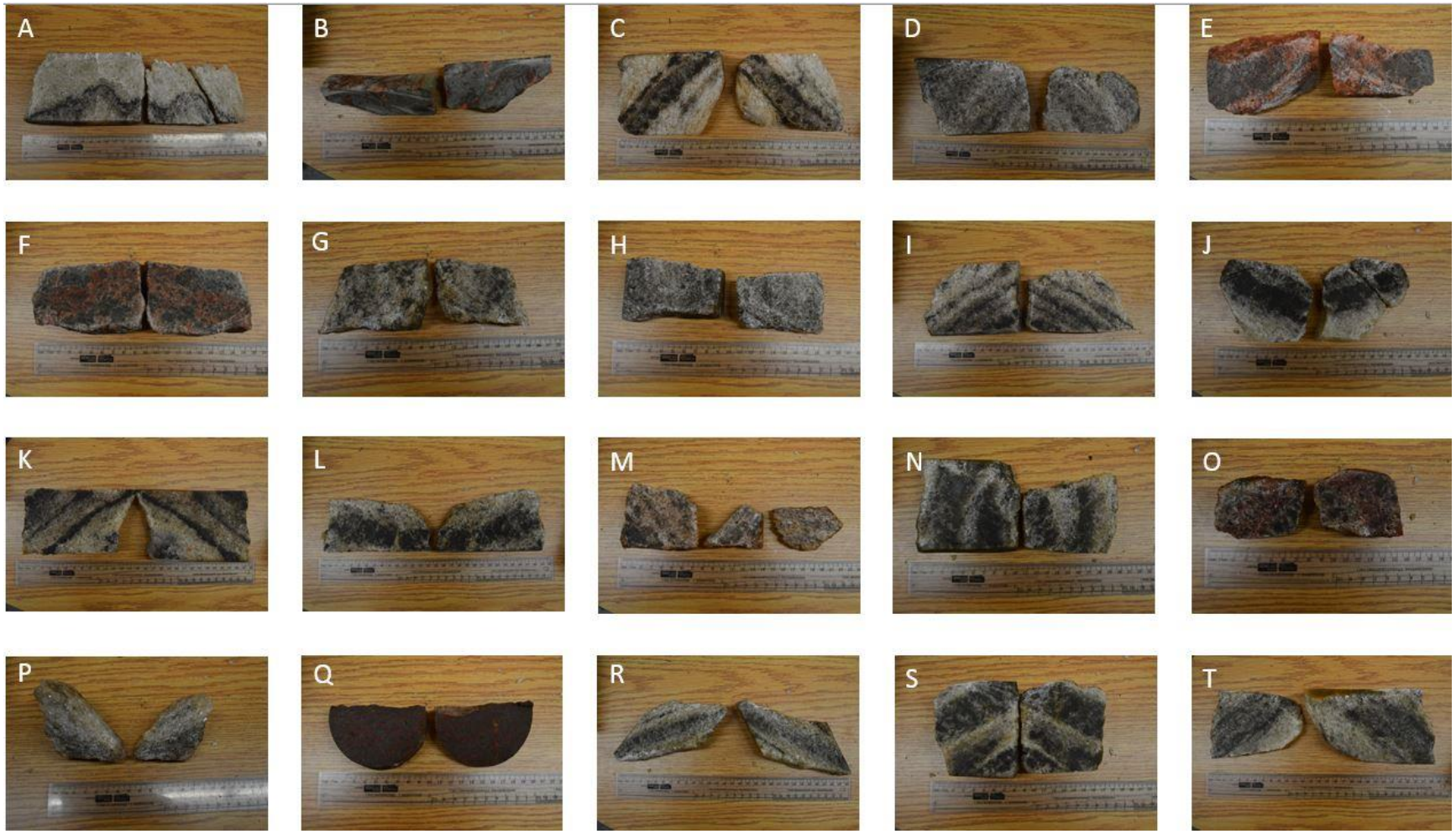

Figure 4.2: Hand Samples cut with a wood saw photographed under plain light. (A) Sample NG-42 from 860 m depth. (B) Sample NG-40 from 875 m depth. (C) Sample NG-39 from 880 m depth. (D) Sample NG-37 from 886 m depth. (E) Sample NG-38 from 890 m depth. (F) Sample NG-34 from 912 m depth. (G) Sample NG-32 from 935 m depth. (H) Sample NG-29 from 950 m depth. (I) Sample NG-27 from 961 m depth. (J) Sample NG-25 from 964 m depth. (K) Sample NG-22 from 993 m depth. (L) Sample NG-30 from 1013 m depth. (M) Sample NG-03 from 1026 m depth. (N) Sample NG-01 from 1038 m depth. (O) Sample NG-18 from 1049 m depth. (P) Sample NG-11 from 1059 m depth. (Q) Sample NG-13 from 1071 m depth. (R) Sample NG-14 from 1102 m depth. (S) Sample NG-08 from 1147 m depth. (T) Sample NG-10 from 1158 m depth.

4.3 Petrographic Description

These thin sections were then described under transmitted light, looking at anhydrite crystal clusters, aiming to discern primary textures. A draping texture, known as snow-on-the-roof texture, was observed (Figure 4.3). This texture is indicative of halite crystals that were growing in a restricted marine environment, before an incursion occurred or temperature changed, changing the seawater chemistry or brine conditions slightly, causing precipitation of anhydrite briefly before the waters returned to their prior seawater chemistry and precipitated a new sequence of halite (Raup & Hite, 1992; Stewart, 1963). As anhydrite grains precipitated out of the water column, they settled out and blanketed the halite present on the basin floor. This texture is represented in stacked sequences within several of the thin sections.

At first, I thought this texture may have been secondary, with anhydrite grains precipitating along halite grain boundaries in association with deformation. However, upon examining the deformed thin sections, anhydrite grains were seen spread throughout the thin section, showing no preferred orientation (Figure 4.3). In addition to this reworking of anhydrite crystals, there were also instances of an overprinted alteration texture in some thin sections, both in obviously deformed sections and seemingly undeformed ones.

This gave the indication that the snow-on-the-roof texture was primary, indicating that primary seawater geochemistry and element concentrations might be retained within these anhydrite crystals. These same snow-on-the-roof textures were also seen by Holt et al. (2014) in their undeformed halite samples from the Pennsylvanian Paradox Formation (Utah, USA).

The snow-on-the-roof texture seen from samples in the Paradox Formation are visible in hand samples, whereas the texture is only obvious in thin section within my samples. This could

indicate that the same processes that caused the snow-on-the-roof texture in the Paradox Basin were occurring within the Cumberland Basin, but on a smaller scale. This indicates that there was some factor that limited crystal growth within the basin, inhibiting the development of large scale snow-on-the-roof textures.

Fluid inclusions were also observed under transmitted light microscopy in halite and anhydrite crystals. Within the halite crystals the fluid inclusions were concentrated along grain boundaries and were generally a part of elongated inclusion trails, illustrating their migration pathways and altered nature (Figure 4.4). The inclusions within the anhydrite crystals are both mineral and fluid (Figure 4.4). The inclusions within anhydrite do not exhibit any obvious alteration and look relatively undisturbed, which helped me to infer that they had a higher potential of retaining primary information in regards to the seawater chemistry and crystallization process.

Reflected light microscopy aided in the identification of any sulfides present. However, there were very few areas of interest located. Nonetheless, this helped to narrow down areas of interest for sampling to obtain information about trace metals in the anhydrite crystals.

Combining the data received from hand sample and petrographic descriptions, I chose specific thin sections that I was interested in studying and determined specific localities within these thin sections that showed the best promise to provide primary element concentrations. These localities were then analyzed using the Electron Microprobe (EMP) (Figure 3.3).

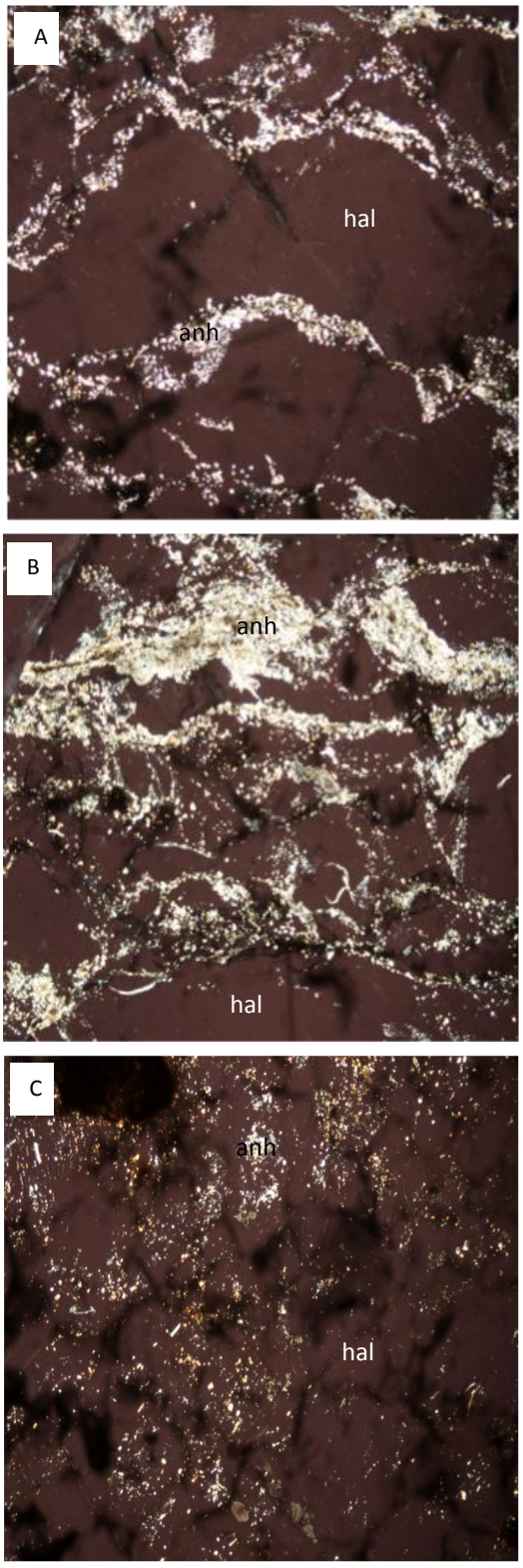

Figure 4.3: (A & B) Thin section photograph in XPL illustrating primary snow-on-the-roof texture, where coarse, angular, bottom-growth halite crystals are draped by anhydrite crystals that precipitated out of the water column and settled on top of pre-existing halite crystals (1 cm fov). (C) Thin section photograph in XPL illustrating secondary recrystallized anhydrite crystals in a halite matrix. The anhydrite crystals after recrystallization are spread throughout the thin section, showing no preferred orientation and not concentrating along grain boundaries. This is a secondary texture (1 cm fov).

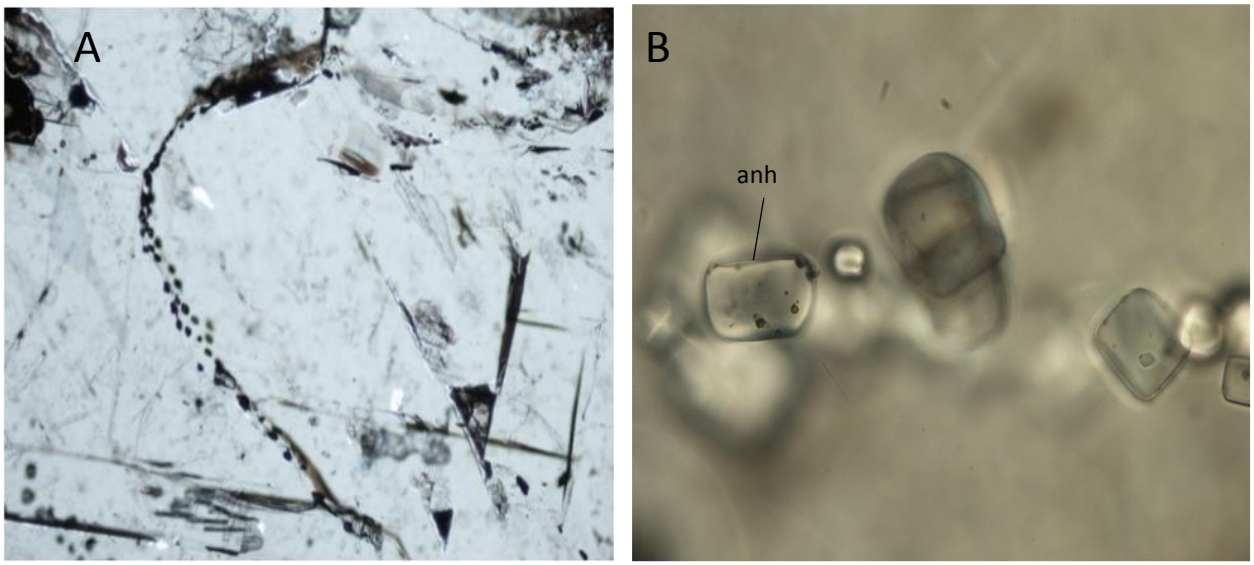

Figure 4.4: (A) Thin section photograph under PPL illustrating altered fluid inclusions that are concentrated in fluid inclusion trails along halite grain boundaries (4 mm fov). (B) Thin section photograph under PPL illustrating mineral and fluid inclusions within anhydrite crystals located within areas of snow-on-the-roof texture (0.5 mm fov).

4.4 Electron Microprobe Analysis (EMPA) Description

The BSE images taken using the EMP helped to reaffirm many of the textures observed in thin section. Snow-on-the-roof textures were seen in many of the less altered samples (Figure 4.5), whereas the obviously deformed samples exhibited anhydrite crystals that were spread throughout the thin section. Additionally, fluid inclusions within halite burst when sealed in the vacuum chamber, creating a condensate and showing their inclusion trail orientation. Likewise, the fluid inclusions within anhydrite also burst, creating a condensate on the mineral surface (Figure 4.5).

With the help of the BSE images, dissolution features were also found (Figure 4.5). These features depict a situation where a snow-on-the-roof texture would have existed, but halite was later dissolved and reprecipitated, moving around the anhydrite crystals. The fact that the halite dissolved, but the anhydrite grain cap was not altered indicates that the deformation conditions did not dissolve anhydrite, possibly illustrating their primary nature.

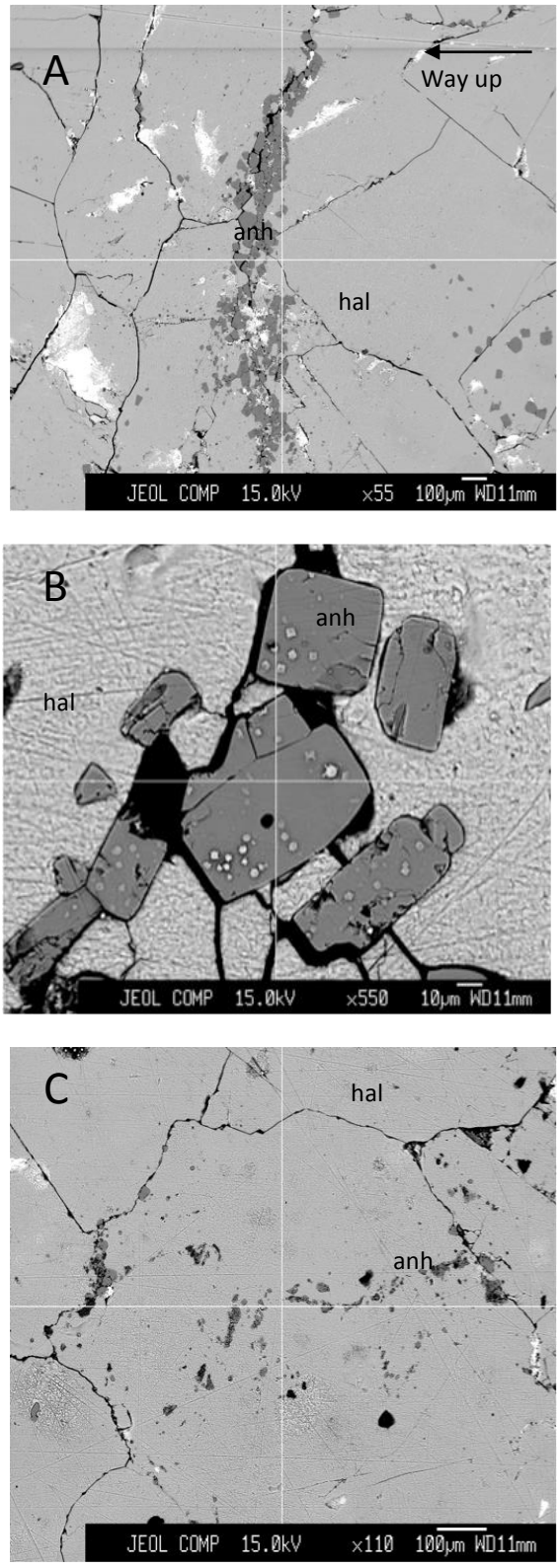

Figure 4.5: (A) BSE image taken using EMP illustrating primary snow-on-the-roof texture preserved. (B) BSE image taken using EMP illustrating anhydrite crystals within a snow-on-the-roof texture, with burst fluid inclusions having formed a condensate on the mineral surface. (C) BSE image taken using EMP illustrating dissolution of halite, reprecipitating around unmoved anhydrite crystals in a preserved snow-on-the-roof texture.

5.0 Results and Discussion

5.1 X-ray Fluorescence (XRF) Analysis

Data was collected from 27 samples that were created through crushing areas of interest into a fine powder using a pestle and mortar. A standard was run prior to my samples to ensure the XRF was working properly. Furthermore, every fifth sample was run twice to ensure that the data collected had acceptable precision. In addition to running samples throughout the core, some areas with clear and dark halite bands were sampled selectively, sampling the clear and dark halite bands separately, with the intent of deciphering the element partitioning that caused this banding. The samples were run twice, once under a custom mode created to analyze elements of specific interest to my study and to give qualitative data about the relationships between my elements and once using a standard method that was already calibrated to give more accurate quantitative values. Magnesium and Br were not part of the suite of elements detected through the standard method, so there values were calculated from Ca and Cl respectively. This was done using correction factors calculated between the first and second run of Ca and Cl values. Na was unable to be measured using the XRF, but the data collected was not normalized to 100% and Na was therefore able to be inferred as the missing data. The collected data (see Appendix C) encompassed many elements that were not studied, or below the detection limit, so a simplified table was created to represent the data used (Table 5.1).

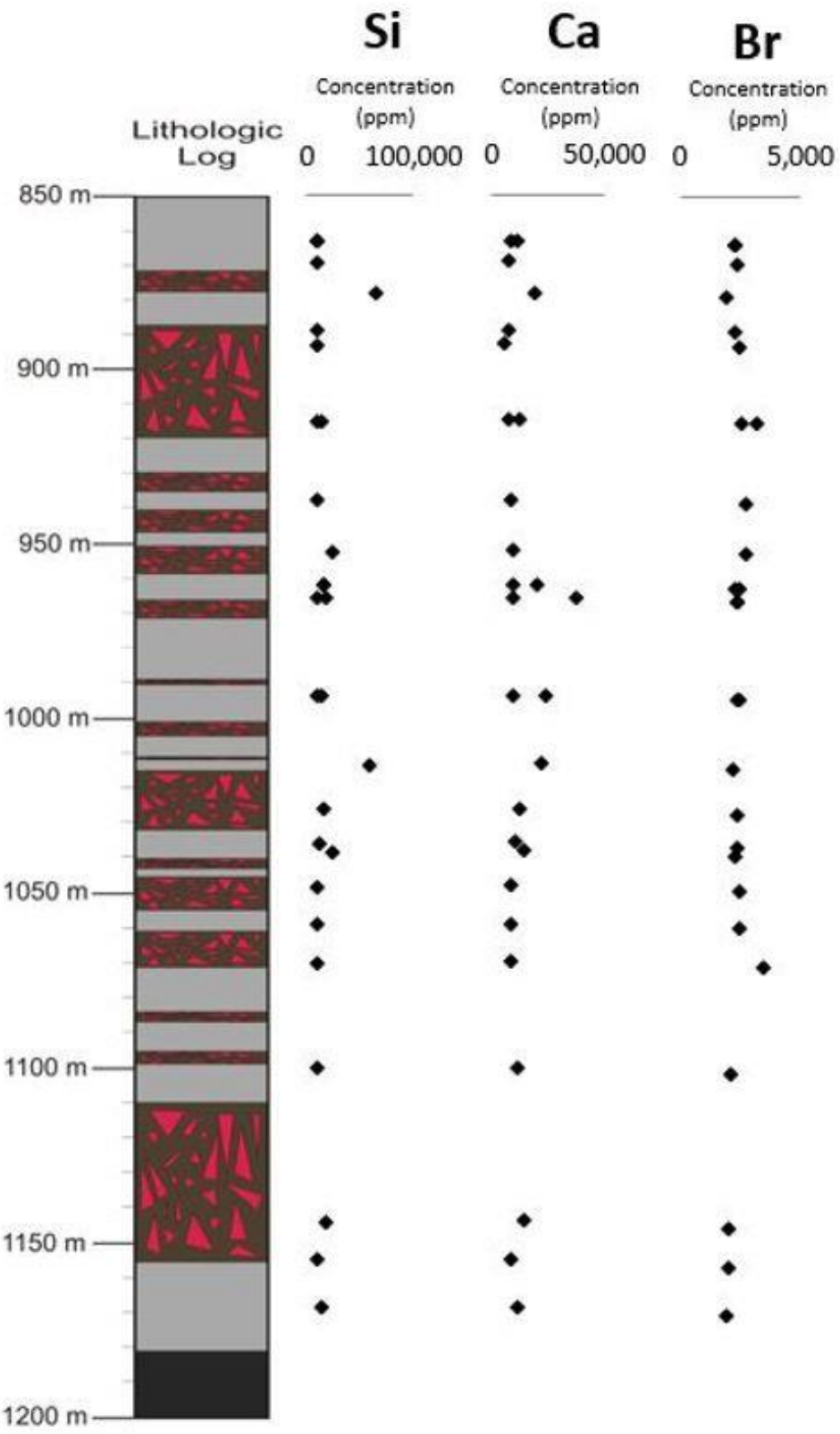

Figure 5.1: Lithologic log with Si, Ca and Br concentration with depth plots to illustrate the location of data points on the core. Si is used as a representation of mud, clay or silt input, Ca is used as a representation of sulfate content and Br is used as a representation of seawater concentration within the restricted basin.

Depth (ft)	Depth (m)	SAMPLE	Fe	Al	Si	Ca	S	Sr	K	Ba	Cl	Mg	Br	Bal	Na
2822	860	NG42-1-C	0.00	0.00	0.00	6470.48	5970.06	6.02	0.00	71.94	437803.42	696.85	1862.99	549452.50	450547.50
2822	860	NG42-2-D	233.36	0.00	0.00	3391.90	3244.80	5.67	0.00	91.60	448706.94	599.38	1819.03	544091.13	455908.87
2841	866	NG41-1	0.00	0.00	0.00	2677.53	2379.61	3.86	0.00	64.81	449176.88	566.17	1890.75	545471.44	454528.56
2872	875	NG40-1	9576.64	13749.65	54003.41	14243.76	14875.35	30.13	9276.04	161.59	334191.66	547.14	1507.59	548430.13	451569.87
2907	886	NG37-1	274.81	0.00	0.00	2654.62	3209.11	4.84	0.00	128.09	453773.91	553.50	1845.98	539635.75	460364.25
2921	890	NG38-1	235.80	0.00	0.00	1023.71	583.20	2.15	0.00	95.22	451795.93	346.16	2044.67	546028.29	453971.72
2994	913	NG34-1-C	728.88	0.00	4374.73	7306.39	6828.04	15.38	7691.09	91.14	423751.50	691.25	2066.00	546422.19	453577.81
2994	913	NG34-2-D	310.48	0.00	0.00	2564.40	2224.37	6.49	73794.41	127.35	423567.59	259.95	2716.59	497032.41	502967.59
3070	936	NG32-1	0.00	0.00	0.00	3921.07	4239.40	3.52	0.00	133.86	456475.16	630.53	2273.58	534978.75	465021.25
3119	951	NG29-1	1753.84	3233.26	12679.49	4517.98	4354.27	9.76	1919.41	122.67	431786.47	553.12	2263.90	539057.38	460942.62
3152	961	NG27-1-C	876.92	1616.63	6339.75	4219.53	4296.84	6.64	959.71	128.27	444130.82	847.35	2050.51	537018.07	462981.94
3152	961	NG27-2-D	1297.14	0.00	5714.57	15135.90	16118.45	23.06	899.42	104.33	423883.50	708.15	1818.76	533673.13	466326.87
3164	964	NG25-1-C	0.00	0.00	0.00	4110.81	3616.40	3.40	0.00	100.53	420451.34	646.59	1954.27	571527.94	428472.06
3164	964	NG25-2-D	1305.51	2798.53	7719.56	32782.45	35492.38	41.52	1251.31	135.10	396751.66	763.52	1940.68	521265.78	478734.22
3258	993	NG22-1-C	89.30	0.00	0.00	4323.88	3821.46	3.87	150.25	110.13	449952.13	707.74	1913.84	541311.13	458688.87
3258	993	NG22-2-D	697.41	1399.27	3859.78	18553.17	19656.92	22.70	700.78	122.62	423351.90	1877.17	2027.29	531288.46	468711.55
3324	1013	NG30-1	5325.19	14134.18	48143.17	17224.71	16289.42	29.33	7568.35	132.10	352590.34	590.28	1782.67	537068.63	462931.37
3367	1026	NG03-1	961.36	0.00	4483.77	7145.03	6745.84	6.79	835.62	102.68	419945.38	618.80	1891.44	559400.81	440599.19
3399	1036	NG02-1	622.59	0.00	1386.09	5550.40	5444.99	6.18	673.59	122.06	435687.59	672.06	1954.57	547639.00	452361.00
3408	1039	NG01-1	2352.58	4686.96	14321.23	9416.85	9030.14	11.78	2650.72	99.84	410622.78	645.03	1813.88	546216.06	453783.94
3441	1049	NG18-1	603.07	0.00	0.00	3373.84	2583.47	4.98	185.22	151.74	443976.59	497.38	2031.24	548780.88	451219.12
3477	1060	NG11-1	116.04	0.00	0.00	3407.37	3294.01	3.79	0.00	92.02	455386.69	648.14	2028.67	522903.03	477096.97
3514	1071	NG13-1	359.56	0.00	0.00	3390.61	2938.74	4.39	92.61	121.88	449681.64	45.04	3024.56	535841.96	464158.05
3616	1102	NG14-1	201.89	0.00	0.00	6278.36	4701.64	5.63	0.00	70.94	453506.59	708.19	1702.42	534952.56	465047.44
3763	1147	NG08-1	1050.16	0.00	7039.31	8911.44	9076.83	7.21	1501.14	89.13	429276.97	671.73	1576.59	540299.44	459700.56
3800	1158	NG10-1	85.93	0.00	0.00	3219.32	3366.32	1.96	1416.49	120.24	457603.91	576.49	1581.76	533945.75	466054.25
3846	1172	NG04-1	568.05	0.00	3519.66	6065.38	6221.58	4.59	1458.82	104.69	443440.44	515.91	1506.55	537122.60	462877.41

Table 5.1: Data table illustrating data collected from the XRF. Sample numbers denoted with (-C) or (-D) indicate clear or dark halite bands measured and Bal indicates the total of all measured elements. All data are in ppm.

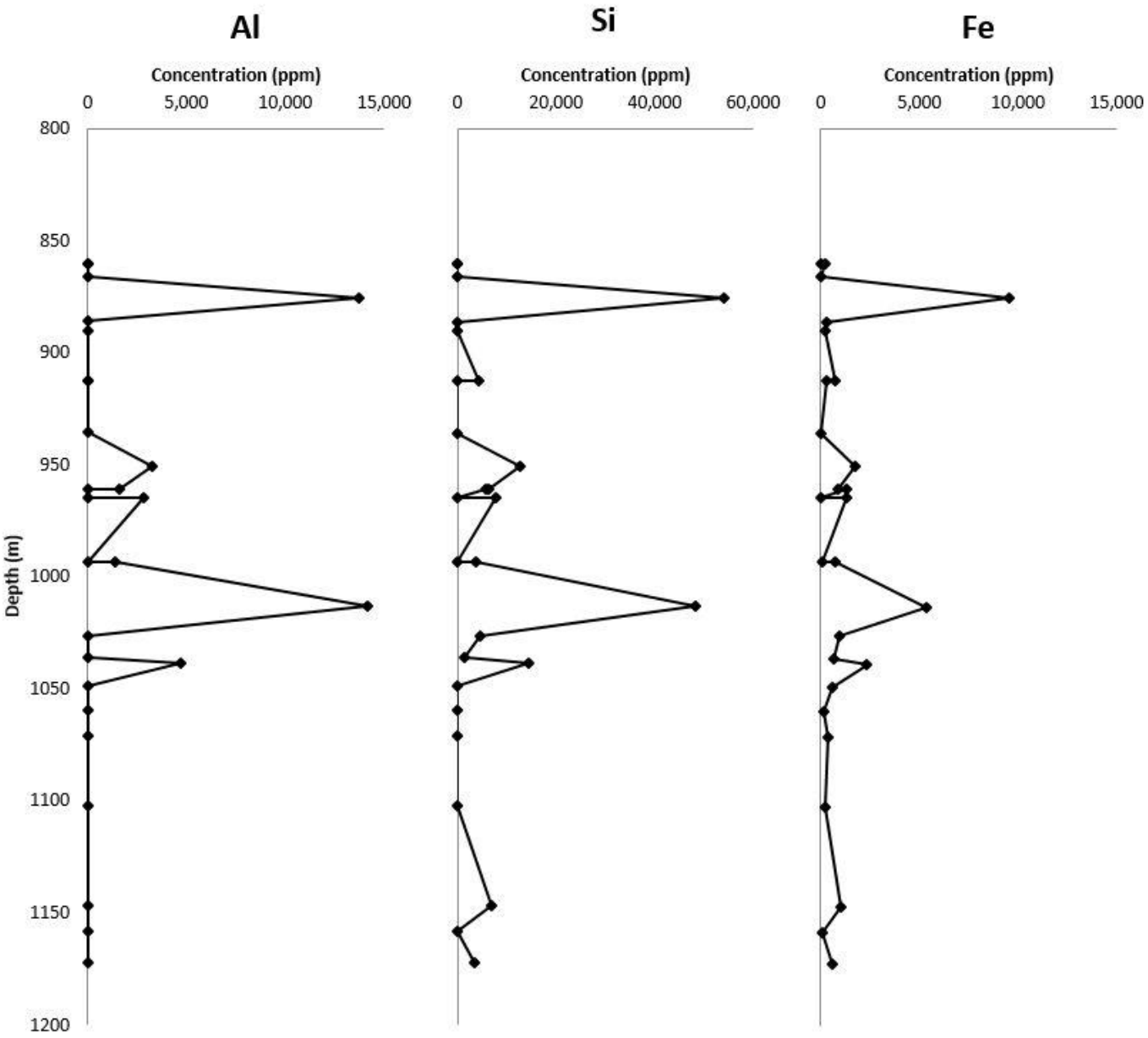

Figure 5.2: Combination of graphs illustrating element concentration in ppm plotted against depth in meters within the core. These graphs show data collected using the XRF and have correlated areas of elevated concentrations.

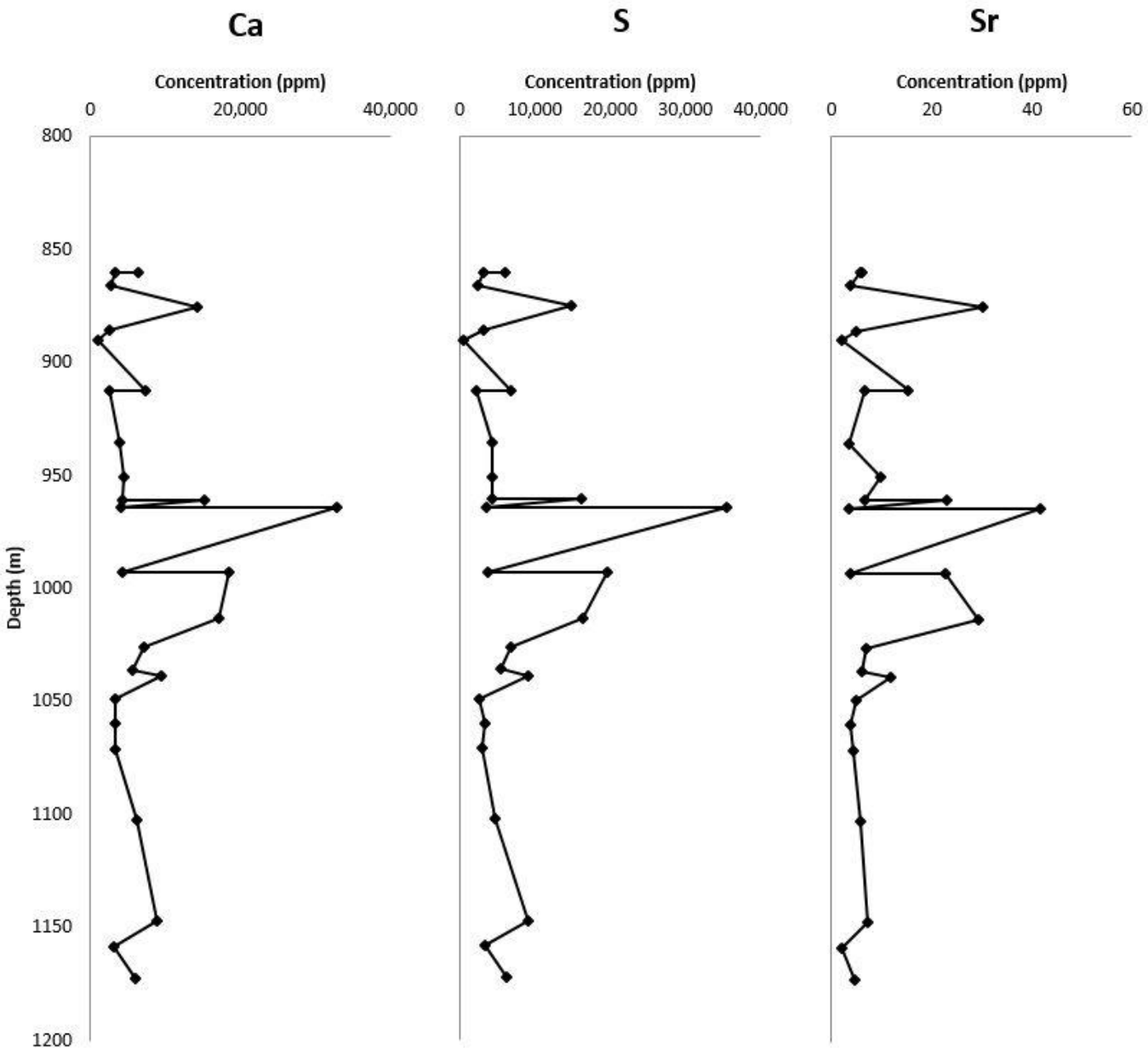

Figure 5.3: Combination of graphs that illustrate element concentration in ppm plotted against depth in meters within the core. These graphs were created from data attained using the XRF and showing a clear correlation in locations with elevated concentrations.

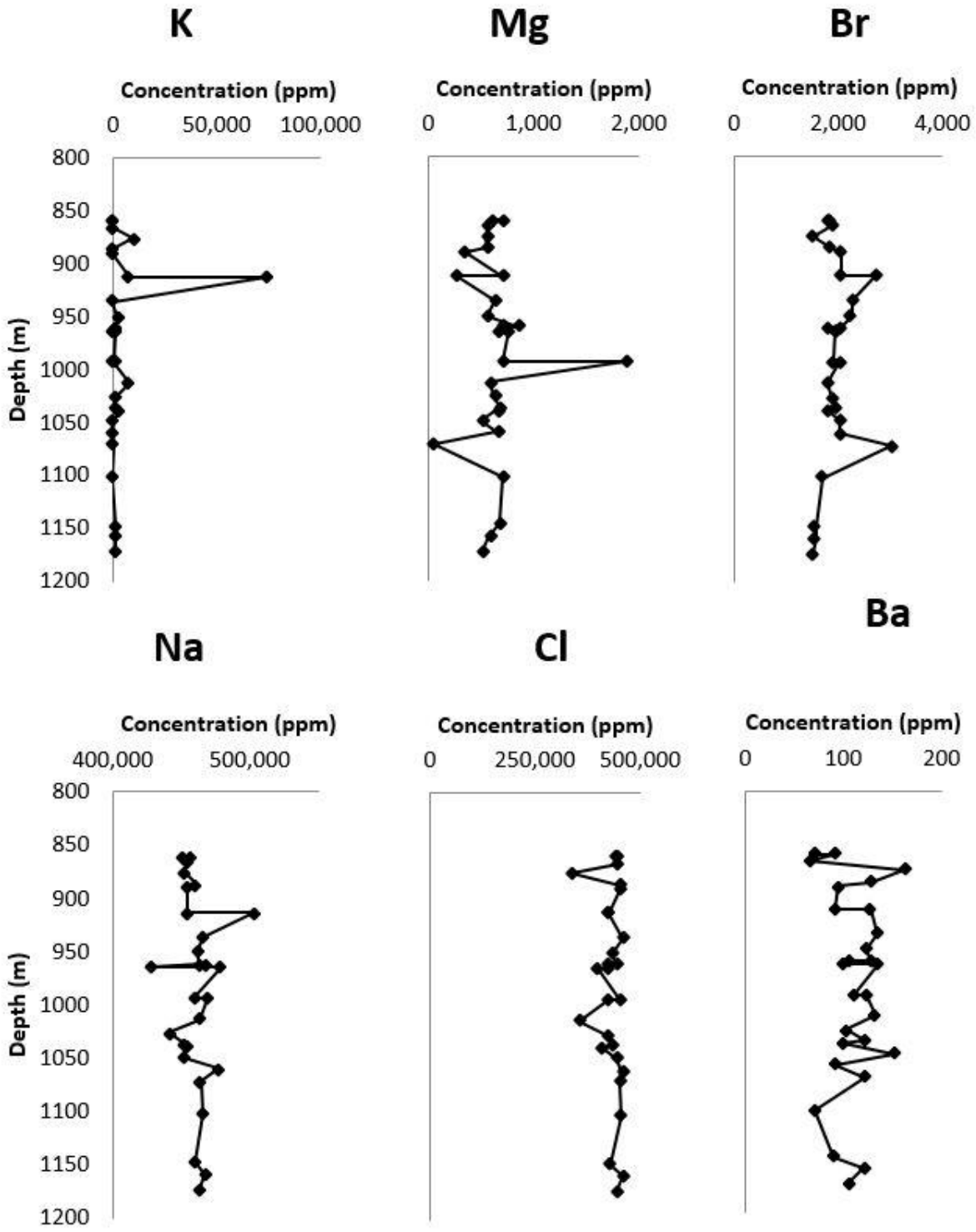

Figure 5.4: Combination of graphs illustrating the element concentration in ppm against the depth in meters within the core. The above graphs represent data collected using the XRF.

5.2 XRF Data Relationships

The XRF data provides a coarse representation of the relationships between certain element concentrations and the mineralogy and deformation seen within the samples (Figure 5.1). Certain elements behave similarly, while certain samples show changes in concentration across all elements, indicating a specific event or shift that occurred.

5.2.1 Element Relationships

Aluminum, silica and iron have the same depth profile trends (Figure 5.2). The concentrations are several orders of magnitude different, but the peaks are located at the same depths. Looking further, the depths that show peaks in Al, Si and Fe are all samples that are brecciated, or have preserved mudstone beds. It is these brecciated or mud rich zones that are where Al, Si and Fe are highly concentrated. Therefore, any area with increased Al, Si and Fe concentrations can be assumed to have undergone deformation or have a substantial mud or clay component. Similarly, calcium and sulfur behave identically (Figure 5.3). These are the elements that make up gypsum and anhydrite, which indicates that the peaks seen in Ca and S are areas that have increased levels of sulfate precipitation. Strontium, although at very low concentrations, also mimics the trend of Ca and S, with all peaks matching, due to being commonly substituted for Ca (Figure 5.3). The peaks seen in these three elements are similar to those seen in Al, Si and Fe; specifically at 875 meters and 1071 meters depth. This could indicate that they are products of deformation. Conversely, it could indicate that sulfate precipitation was occurring, and another event such as a rapid input of surface waters caused an influx of sediment that blanketed or disturbed the sulfates. Moreover, the sulfates could

have been precipitating in the late stages of evaporation, persisting in a sabkha-like environment where sediment input was more frequent, creating these mudstone layers.

5.2.2 Depth Relationships

Many elements show peaks at the same depths, indicating that they were being preferentially uptaken or incorporated into the chemical structure of the precipitating minerals at that point. The most obvious example of this is at 1071 meters depth where there are peaks in Al, Si, Fe, K, Ba, Sr, Ca, S and troughs in Mg, Br and Cl (Figure 5.2, Figure 5.3 and Figure 5.4). These peaks and troughs are of varying intensities, with a large drop in chlorine and a drop in bromine concentration potentially indicating brine dilution through seawater input. Mg also shows a drop, potentially indicating that carnallite existed at this locality but was recrystallized as sylvite, leading to a peak in K, after the magnesium was mobilized and removed. The sample from this depth is a mudstone with nodules of sylvite, along with small proportions of halite and anhydrite within the matrix.

Another example exists at 1160 meters, where there are peaks in Ba and Cl, but troughs in S, Ca, Sr, Mg and Fe (Figure 5.2, Figure 5.3 and Figure 5.4). The sample illustrates preserved bedding with a mixture of both clear and dark halite and does not look obviously altered, still having dogtooth halite crystals preserved. This could mean that there was increased halite precipitation at this depth, with a decrease in anhydrite precipitation. The increase in Ba could indicate that there was an influx of surface ocean water, where Ba exists in high concentrations, into the restricted basin. The concentration of barium varies constantly over the length of the core, indicating that it is not a sensitive indicator of rhythmic inputs or climatic trends.

5.2.3 Halite Banding Differences

Five different samples were analyzed specifically looking at clear and dark halite bands (Figure 5.5, Figure 5.6, and Figure 5.7). From this data, it was seen that the darker halite bands generally had higher concentrations of Fe, Al, Si, K, Ca and S. Similar levels of Mg, Ba and Br exist despite the banding seen. The increased amounts of Fe, Al and Si could indicate that deformation is more localized along these dark bands. However, considering the small scale of the bands, this is unlikely. Instead, it is more likely that the dark halite may be attributed to increased amounts of mud, clay or silt, staining the halite a dark grey to black colour. This corresponds to the interbedded black shale seen in the Paradox Formation, which was associated with water level changes within the restricted basin (Raup & Hite, 1992). The increases in calcium and sulfur are also meaningful considering anhydrite crystals can diffuse light, causing the rock to appear a darker colour (Raup & Hite, 1992). The combination of increased siliciclastic sedimentation and increased anhydrite precipitation likely caused the dark banding seen throughout the core.

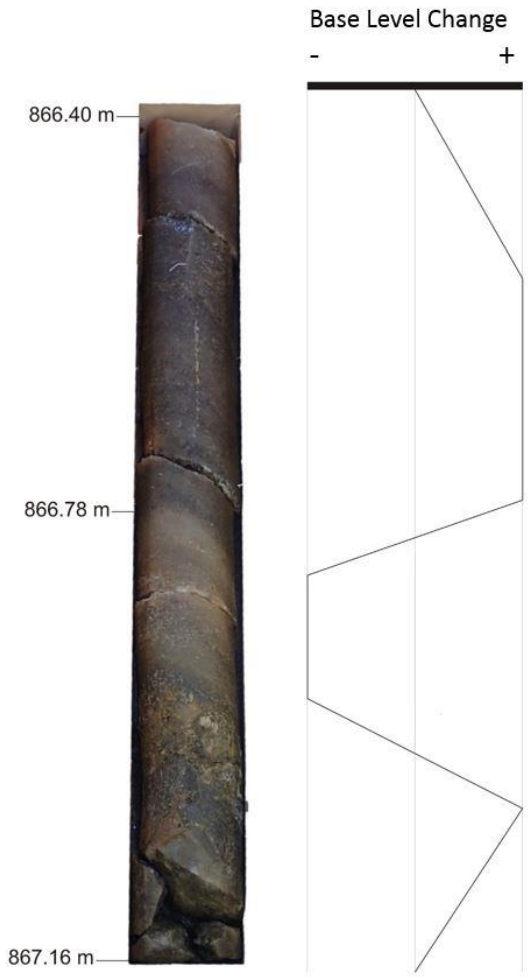

Figure 5.5: Section of core illustrating banded halite annotated to show potential base level change cycles that caused these light and dark halite bands.

The existence of more organic rich siliciclastic rocks and concentrated anhydrite layers indicates the likely preservation of similar cyclic changes in base level described within the Paradox Formation (Figure 5.5 & Figure 5.6) (Raup & Hite, 1992) and within the Cumberland Basin by Boehner (1986) and Schenk et al. (1994). These cycles, which vary in thickness and abundance throughout the core can act as an indicator for the magnitude and periodicity of inflow into this restricted basin. The scale on which these halite bands were analyzed cannot confirm this hypothesis, as changes in the concentration of Ca, S, Fe, Al and Si cannot be measured across the width of the halite bands, instead only showing an increase across the entirety of the dark bands.

Figure 5.6: Section of core illustrating banded halite annotated to show potential base level change cycles that caused these light and dark halite bands.

More fine scale measurement of several points across these dark bands could better constrain the nature of these cyclic base level changes and confirm if in fact this is what caused the banding. Furthermore, the increase in Fe, Al and Si is not consistent across all samples and is quite small in some samples, making further study of these bands important in confirming this hypothesis. Additionally, samples taken from dark bands were predominantly crystalline, avoiding mud rich zones in an attempt to isolate changes within the crystals themselves. This

sampling method would produce an understated Fe, Al and Si concentration when considering the entirety of the dark halite band.

The increase in K within these areas indicates increased sylvite precipitation, which is confirmed through hand sample identification. At 913 meters depth, where there is a large spike in the potassium concentration, it should be noted that this band contained dark halite, but also sylvite crystals that were clearly visible in hand sample and under UV fluorescence. Other samples showed spikes in K concentration, but not to a degree that was determined significant for further analysis.

When looking at chlorine levels in the clear and dark bands, an inverse trend is seen, with the clear halite generally having higher chlorine levels than the dark halite (Figure 5.7). This drop in chlorine concentration within the dark bands matches what Raup and Hite (1992) proposed regarding these dark bands being physical representations of cyclic base level change

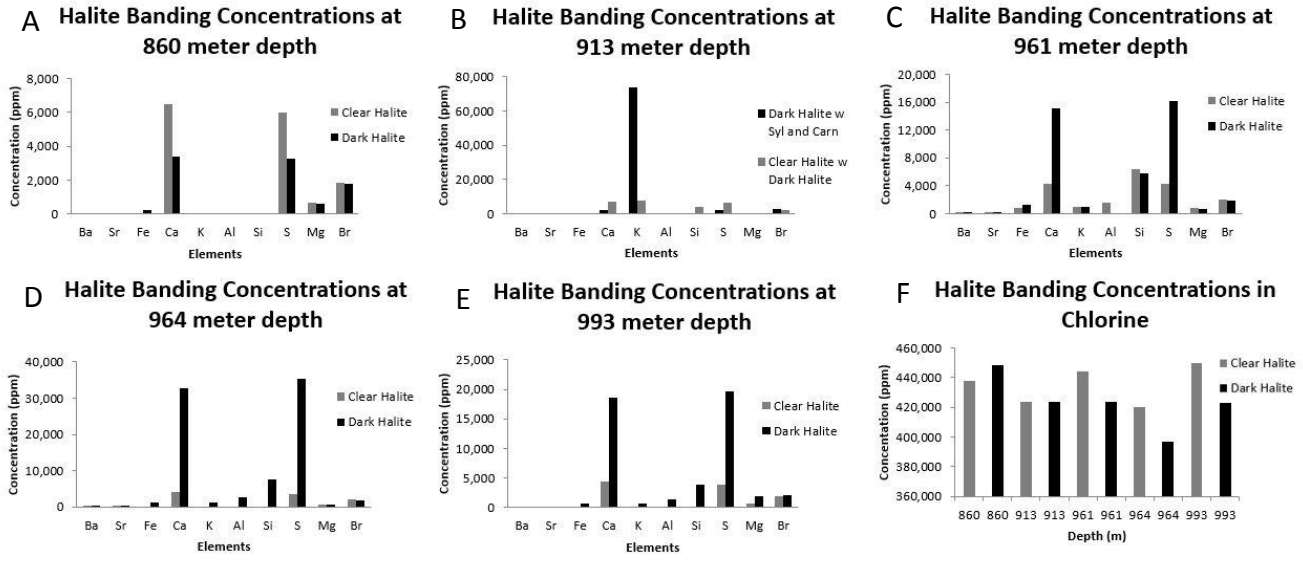

Figure 5.7: A. Illustrates the clear and dark halite band element concentrations at 860 meter depth. B. Illustrates the clear and dark halite band element concentrations at 913 meter depth. C. Illustrates the clear and dark halite band element concentrations at 961 meters depth. D. Illustrates the clear and dark halite band element concentrations at 964 meters depth. E. Illustrates the clear and dark halite band element concentrations at 993 meters depth. F. Illustrates the chlorine concentrations within the clear and dark halite bands at varying depths.

within the restricted basin. Changes in sea level, which affected the Pennsylvanian Paradox Basin (Raup & Hite, 1992), could have occurred within the Mississippian Cumberland Basin as well, or these cyclic base level changes could be representative of basin recharge due to storm events or seasonal input.

The presence of brecciated material within these banded areas and elsewhere in the core could also be indicative of these storm or input events, where there would have been the potential for reworking of recently deposited evaporites and sediments, creating primary clastic material that is hard to decipher from brecciation that occurred during halokinesis. This matches what can be expected in relatively deep evaporite basins where turbidites and mass flows can occur (Warren, 1989).

5.2.4 Element Ratios

Specific elements have characteristic ratios that can help determine climatic and temperature changes (Figure 5.8). If these ratios are relatively consistent, it generally means that the environment that the elements existed within was maintained, with little change in temperature, water inputs and seawater chemistry. The ratios I looked at were Mg/Ca, Sr/Ca and Br/Cl. The Mg/Ca ratio depicts the amount of surface seawater water input present and also the source and temperature of the seawater. The Sr/Ca ratio is relatively well constrained and constant throughout the ocean, therefore allowing the determination of how recently the restricted basin had an inflow of seawater to be quantified, based on the variation from this well-known ratio. The Br/Cl ratio indicates whether seawater concentrations have been maintained or whether they have been altered through hydrothermal processes. The Br/Cl ratio

specifically takes into account the frequency with which bromine substitutes for chlorine within the halite structure. This occurs at a constant and defined rate, which is why it can be used.

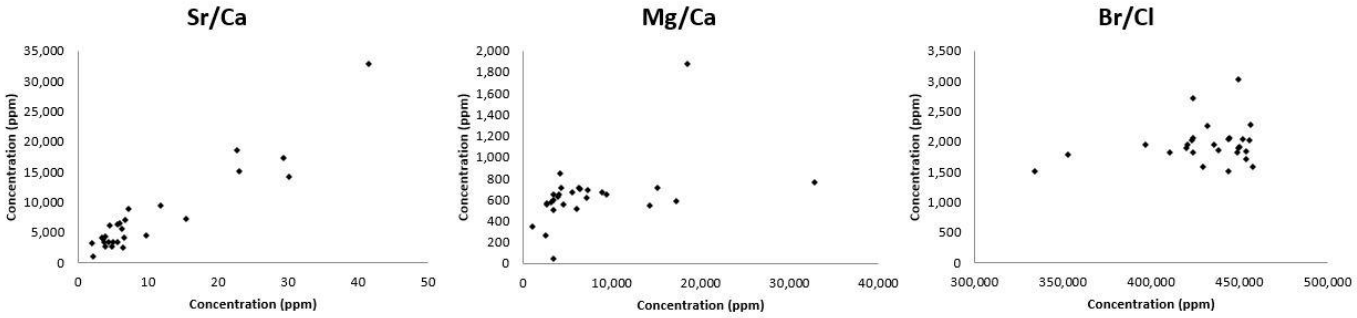

Figure 5.8: Graphs illustrating ratios for the whole rock analysis acquired from the XRF.

The ratios calculated through my study are relatively consistent, which support the conclusion that the basin was relatively stable, with occasional influxes of seawater into the system. Outliers could indicate localized changes that occurred, or areas where deformation has changed the ratios. Given a lack of distribution coefficients helping to detail how frequently substitutions of certain elements occur, a quantitative assessment of these ratios cannot be

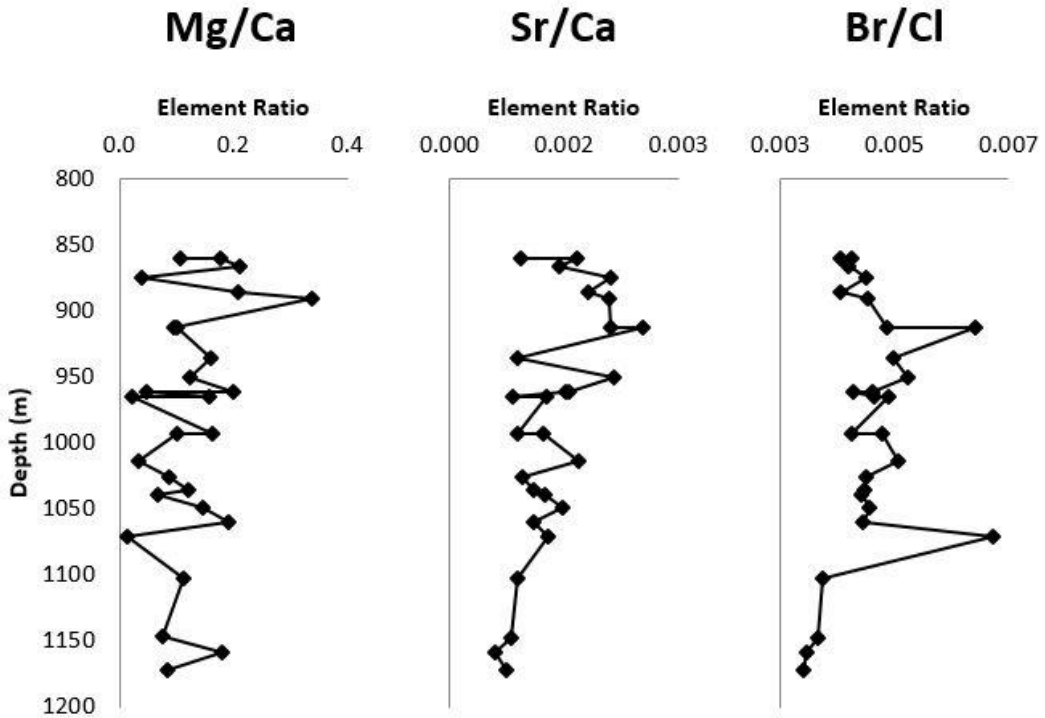

Figure 5.9: Element ratio vs. depth graphs for Mg/Ca, Sr/Ca and Br/Cl.

completed. These ratios can also be plotted against depth to provide information about their change throughout the extent of precipitation (Figure 5.9).

5.2.5 Bromine Concentration

The bromine concentrations generally increase as you move from the bottom to the top of the deposit, with two distinct dips that likely indicate a significant marine incursion which diluted the brine and caused a reduction in salinity and also a reduction in the concentration of bromine (Figure 5.4). This trend matches that seen within the Paradox Formation, where the bromine is used as an index for the concentration and salinity of the brine (Raup & Hite, 1992). The increasing trend indicates that the brine within the restricted basin was becoming more concentrated as more evaporation and subsequent evaporite precipitation occurred. The regular nature of this trend indicates that the Wallace Sub-basin had to be relatively large to accommodate a large volume of brine that would not be largely effected by small marine inputs. This regular profile contrasts with what would be expected from a small basin with frequent episodes of marine input and recrystallization, which would cause a jagged irregular trend (Raup & Hite, 1992).

Additionally, the steady trend seen in bromine concentration indicates nearly continuous precipitation throughout the life of the basin (Raup & Hite, 1992). This factor indicates that the basin would have had to be at least as deep as the thickness of an entire halite bed (Raup & Hite, 1992), which cannot be quantified confidently due to the diapiric nature of the Wallace-1 core, but likely varied from 10’s of meters up to 100 meters. These cycles are illustrated through the created lithologic log (Figure 1.2).

5.2.6 Evaporite Precipitation Cycles

The XRF data supports the idea that these evaporites precipitated in a restricted basin with occasional seawater input. The bromine data (Figure 5.4) produces a clear image as to the likely precipitation sequence, with steady evaporation and seawater recharging the basin periodically. The bromine data shows two cycles of increasing concentration, where the evaporation would have been taking place, allowing for brine concentration and thus bromine concentration, before seawater recharged the basin and diluted the brine briefly before evaporation continued and the brine began to concentrate again.

Looking at the finer scale interbeds of clear and dark halite, there were many smaller seawater incursions that caused cyclic base level changes, which are recorded in these dark halite bands.

The peaks in calcium sulfate element concentrations depict a similar cyclic evaporite sequence, with concentrations of Ca increasing as the brine concentrated, then dropping as the basin was recharged. The chlorine concentration is relatively constant, roughly matching the trend of bromine, indicating that halite precipitated throughout the life of the basin, helping to constrain the brine concentration and evaporation extent.

The peaks in potassium concentration seen in several areas of the core, mainly being focused near to mudstone dominated areas could indicate that their precipitation occurred during late stage evaporation under extreme brine concentration. The precipitation of sylvite followed by mudstone beds could indicate the basin was experiencing increased sediment input due to reduction in brine volume, potentially in a sabkha environment (Warren, 1989). As suggested by Raup and Hite (1992), this indicates an arid climate persisted at the time.

5.3 Electron Microprobe Analysis (EMPA)

Data was collected from 17 thin sections that were created from samples collected from the DNR Core Warehouse in New Glasgow, NS. The original samples that were made into thin sections were chosen based on quality, but also based on their depth, aiming to illustrate the entirety of the core as best as possible. The 17 thin sections that were chosen for microprobe analysis range in depths from ~850-1190 meters and were analyzed for Na, Cl, Ca, S, Sr, Br, Mg, Ba, P and K. Once this data was collected, I averaged all of the element data for each thin section after removing any data points that were below the detection limit, so as not to skew the data. After this, I plotted the data to show concentration changes with depth to help illustrate any trends or similarities between my data.

All data collected was in oxide weight percentages (see Appendix D), but was converted to ppm, which is how it is presented, to make comparisons with data collected from the XRF easier (Table 5.2).

5.4 EMPA Data Relationships

The EMP data was collected mainly on anhydrite crystals with the intent of using their more robust nature, being less soluble with increased temperature, to determine primary seawater geochemical features. This data provided in depth and accurate information about the trace elements incorporated into anhydrite crystals (Figure 5.10). Anhydrite crystals within areas exhibiting primary snow-on-the-roof textures were focused on, with the understanding that these preserved textures gave a better likelihood of obtaining preserved primary geochemical data.

The EMPA was also completed to supplement data obtained through XRF, giving a more well-rounded understanding of the whole rock and the finer-scale mineralogical changes that took place within the restricted basin.

5.4.1 Element Relationships

In contrast to the data collected with the XRF, similar trends are not as obvious between specific elements from the EMP data. There are still similarities between calcium and sulfur in terms of peak and trough locations, but between these peaks and troughs the elements behave differently, likely due to element substitution, which is not registered as obviously when analyzing the whole rock composition. Sodium and chlorine also show similar trends in their concentration with depth, with peaks and troughs occurring at similar localities.

5.4.2 Depth Relationships

When looking at concentration changes with depth, there are several instances where correlations between specific elements can be made (Figure 5.10). Starting at the shallowest depth, both Na and Ba show peaks at 860 meters. At 875 meters depth, K and Mg have large peaks, which is interesting considering the rest of the EMP data and XRF data show Mg being low throughout the section. The sample taken at this depth is highly brecciated, but unlike other samples concentrated magnesium levels, potentially indicating the presence of carnallite. At a depth of 890 meters, Na and Cl have peaks, while S, Sr, K, Mg and Ba all experience large troughs. At a depth of 913 meters, S has a peak and Na and Cl have troughs. Furthermore, Ca and S experience peaks at 1039 meters; K shows a peak and Sr shows a trough at 1039 meters; Na shows a peak at 1049 meters and Cl shows a trough at the same depth; Ca and S both have peaks at a depth of 1102 meters, whereas Na has a trough at this depth; Na, Ba and K both

Depths (ft)	Depths (m)	Sample	Ca	S	Sr	Na_2	Cl	Mg	K_2	Br	Ba	P_2
2822	860	NG43	278954.87	232220.47	306.29	450.32	1363.33	61.81	179.34	243.75	0.00	177.48
2822	860	NG42	280197.61	231430.95	543.41	656.61	1193.60	65.79	132.40	286.25	428.12	182.38
2872	875	NG40	279987.91	231590.92	259.32	340.98	1641.43	206.54	392.59	268.33	0.00	90.56
2907	886	NG37	289627.04	232336.20	398.28	426.98	1371.54	63.92	50.74	291.00	0.00	84.01
2921	890	NG38	287526.91	227689.46	0.00	852.90	3850.00	0.00	91.33	0.00	0.00	209.49
2994	913	NG34	281770.50	233159.17	260.44	317.34	320.00	69.95	71.96	123.33	0.00	59.65
3119	951	NG29	281729.98	232658.35	329.78	598.30	2226.67	102.52	114.16	245.00	0.00	186.79
3152	961	NG27	278423.93	232616.97	341.76	421.78	1219.33	50.66	163.68	216.67	200.03	108.62
3164	964	NG25	280451.18	231621.38	310.99	336.81	1268.33	41.01	123.50	188.57	8.96	181.32
3258	993	NG22	281740.71	230372.15	249.45	449.79	1701.67	82.42	69.19	306.67	201.52	123.65
3324	1013	NG30	288830.74	233173.66	494.67	504.95	1390.00	18.09	69.19	506.67	0.00	93.83
3408	1039	NG01	284735.71	230268.69	109.93	570.72	1706.67	84.43	260.15	320.00	0.00	198.58
3441	1049	NG18	287774.01	229968.76	424.01	664.08	2057.78	63.32	153.00	440.00	0.00	123.65
3477	1060	NG11	282063.69	231119.76	287.50	463.05	992.50	67.84	71.96	321.43	389.61	108.38
3616	1102	NG14	290953.73	233669.84	247.64	304.10	1031.11	67.54	100.82	567.50	0.00	150.88
3763	1147	NG08	280530.73	230285.21	422.80	511.58	1453.75	97.99	259.75	277.50	134.35	83.79
3800	1158	NG10	275862.35	230654.51	935.79	428.57	1537.78	51.86	153.60	350.00	0.00	120.75

Table 5.2: Data table illustrating data collected from the electron microprobe. All data within this table has been averaged based on sample number and listed against their corresponding depth.

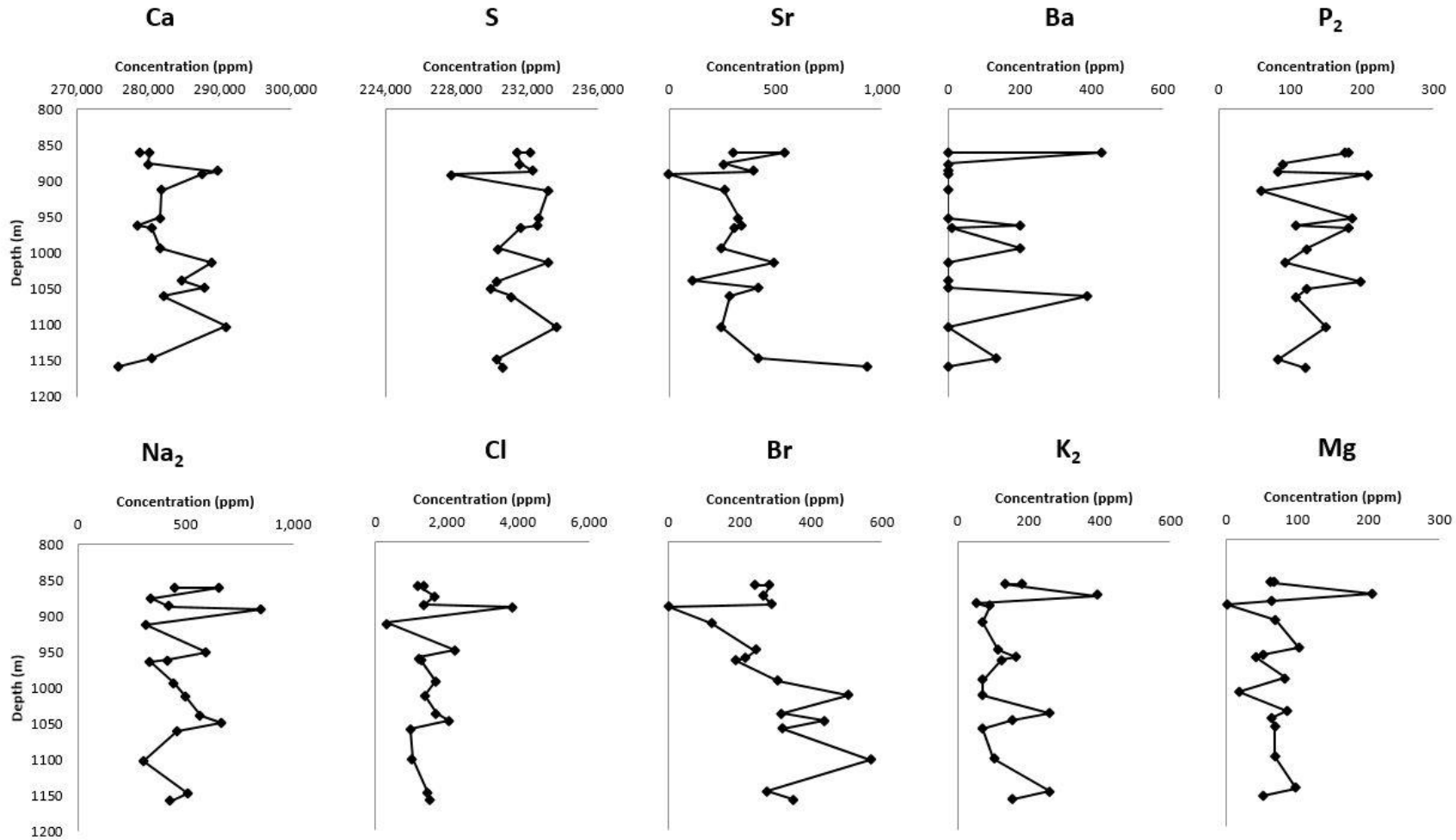

Figure 5.10: Combination of graphs created that plot elemental concentration in ppm against the depth in meters within the core. The Graphs show data collected using the Electron Microprobe.

have peaks at 1147 meters and finally, Sr has a large increasing trend towards 1158 meters, while Ca exhibits a decreasing trend over this same interval. In general, the trends recorded by the anhydrite crystals are not as variable as those exhibited in the corresponding whole rock analysis. This suggests that the anhydrite composition represents similar conditions throughout the measured sequence.

5.4.3 Element Trends

The individual element trends act as a helpful characterization tool to determine finer scale processes within the basin. Calcium and sulfur exhibit cyclic jumps in concentration, owed to their concentration changes within halite banding (Figure 5.10). They would have also been affected by substitutions of other elements into the chemical structure of anhydrite. Changes in Na and Cl help to indicate the dominant mineral precipitating at the time. When Na and Cl values are high in anhydrite, it indicates that less was being used to precipitate halite (Figure 5.10). Chlorine could also be affected by periods of seawater input, diluting the overall concentration. Potassium and Mg slowly increase in concentration from the bottom to the top of the core, but drop sharply near the top of the core when sylvite and carnallite precipitation would have begun, taking up all available K and Mg (Figure 5.10). Strontium is also cyclic and in relatively constant proportions, being quickly substituted into the anhydrite structure. The peaks exhibit areas of seawater input where strontium levels would have risen and the troughs show where the anhydrite has depleted the waters of Sr through substitution with Ca (Figure 5.10). Bromine starts high in anhydrite when the brine would have been saturated with Cl. As the brine became more concentrated and halite precipitation started to take up more Br, there would have been less available to be used in anhydrite (Figure 5.10), creating an inverse

relationship to the XRF (Figure 5.4), which showed an increasing trend. Phosphorous is at very low levels within anhydrite and is highly variable, likely due to cyclic inputs or basin changes, as is similar to many other minerals (Figure 5.10).

5.4.4 Anhydrite Precipitation Cycles

Over the entire extent of the deposit, there is little variation seen within the majority of the elements, especially calcium and sulfur, which make up anhydrite. This indicates that the seawater chemistry must have been relatively consistent for such little variation to be present. This indicates that anhydrite precipitated under restricted conditions within a narrow chemical window. In addition, the cyclic nature seen within the plots is evident of periodic inflows of marine waters, replenishing the system.

This supports the idea that the restricted basin had relatively consistent conditions, with little variations and occasional inputs. The trace elements that were substituted into the anhydrite crystals are also able to be qualified in relation to the nature of the basin and its periodic recharge.

In addition, this supports the idea that despite halokinesis, the original geochemical features have been retained within these anhydrite grains, as well as within the whole rock, allowing for paleoenvironmental conditions to be inferred.

6.0 Conclusion

Based on the collected data, it can be concluded that the Wallace-1 core retains many of its primary seawater geochemical features. Despite the fluid inclusions likely being reset and not providing primary seawater information, the element concentrations and their relationships provide clear information about the paleoenvironment in question.

The preservation of halite banding, indicative of small scale base level changes within the basin, along with the preservation of mudstone bedding, indicative of late stage, shallow marine environments with terrestrial inputs, both show that despite halokinesis primary geochemical features still exist. It also sheds light on the basin dynamics, starting as a relatively deep basin, shallowing into a sabkha-like environment before being recharged, although not to the original depth, due to precipitation outpacing subsidence, with this cycle repeating throughout the life of the basin.

The preservation and abundance of snow-on-the-roof textures that are seen within the thin sections prove that seasonal changes in temperature and/or seawater chemistry were recorded and have persisted despite deformation, aiding in the conclusion that the anhydrite crystals are unaltered in portions of the deposit, showing that the element concentrations are consistent with what they would have been during original deposition. The fact that these textures are apparent on a different scale than in the Paradox Basin could indicate: i) the conditions within the basin did not allow for larger crystal growth; ii) the precipitation was slower, not allowing for larger scale crystals to nucleate and grow; or iii) the cycles could have been more rapid, not giving the crystals enough time to grow to the same size.

The XRF data and the associated trends between related elements indicate that alteration has not largely disturbed the geochemical record maintained within the samples studied despite deformation. Thus, the idea that the Wallace Sub-basin was a restricted, deep to shallow marine basin with occasional marine input, which replenished the basin and diluted the brine, holds true.

The EMP data proves that the anhydrite crystals precipitated under a narrow set of conditions that persisted throughout the entirety of the core, indicating that these strict conditions must have also persisted through the life of the basin. The anhydrite crystals also define cyclic conditions where recharge waters must have flowed into the basin. The anhydrite crystals also give information about the nature of these waters, with the peaks in Ba indicating marine surface water input, increased Sr showing marine inflow, Na and Cl showing halite co-precipitation levels and Mg and K indicating brine concentration and evaporite cycle stage.

The Wallace Sub-basin was located at equatorial latitudes and existed through semi-arid to arid climates, with occasional marine inputs and the potential for meteoric water inputs through runoff or storm events. The basin experienced rapid subsidence, prior to and throughout the course of evaporite precipitation. The precipitation of halite, anhydrite, sylvite and likely carnallite, with additions of mud, clay and silty material, both in low stand and high stand periods, led to the lithologic assemblage seen in the core. The precipitation was rapid and consistent throughout the life of the basin. The basin was cut off either through glacial related sea level drop or tectonic activity. Halokinesis occurred shortly after, during the deposition of the Mabou Group and deformed the salt deposit, causing it to migrate vertically into the cores of salt domes during the late Carboniferous.

Evaporites provide a direct measure of paleoseawater geochemistry. The fluid inclusions within evaporites provide data about the seawater at the time of precipitation. Many other rock types can be used to make inferences or judgements about climatic and oceanographic changes at the time of deposition, but few, if any, can provide the same precise information that evaporite deposits can. Thus, salt domes, which are large bodies of evaporites, are

important tools to study when attempting to reconstruct the climate and seawater chemistry of a specific time period. The determination that primary seawater geochemical signatures can be retained within anhydrite crystals and the whole rock despite deformation processes can be helpful in reconstructing paleoenvironmental conditions. The ability to do this can provide information about temperatures, fresh versus marine water inputs and the frequency of these inputs, as well as helping to identify climatic changes. In areas lacking undeformed salt deposits or other rock types commonly used for making inferences about climate, salt diapirs, which are common throughout Nova Scotia and many areas, can be utilized. These findings are especially important considering evaporite basins of Carboniferous age are rare, making the study of those that do exist of great importance. This is especially true considering the Carboniferous period marked a transition from calcite to aragonite seas. By further studying these deposits, this shift in seawater chemistry, which has occurred several times throughout geologic time, can be better quantified and understood.

If I were to continue this research there are several avenues that could be explored. Firstly, ICP-MS analysis could be completed to determine more quantitatively the variations in the bulk rock geochemistry. This analysis could also be done at a finer scale on the dark halite bands to discern element partitioning within them, helping to determine concretely if they are in fact preserved base level changes. Further microprobe work could also be undertaken to look into the potassic salt concentrations within these samples. Distribution coefficients could be created to help model the evaporation process which precipitated the sequence seen in the Wallace-1 core and give the ability to analyze element ratios in more detail. Sulfur and oxygen isotope data could also be collected to better constrain inputs and environmental conditions.

Finally, fluid inclusion analysis could be completed with the intent of determining the degree to which the fluid inclusions have diverged from original seawater compositions. From this, a study of the deformation and hydrothermal fluids could aid in the understanding of the specific halokinetic processes that occurred in the early Namurian and if any subsequent deformation occurred at a later date. The findings of my study, showing that salt diapirs can retain primary seawater geochemical features, makes exploration of the above future work valuable.

7.0 References

Blakey, R. (2013), North American Key Time-slice paleogeographic Maps. *Colorado Plateau Geosystems, Inc.*

Boehner, R. C. (1986), Salt and potash resources in Nova Scotia, *Department of Mines and Energy*.

Calder, J. H. (1998), The Carboniferous evolution of Nova Scotia, *Geol. Soc. London, Spec. Publ.*, *143*, 261–302.

Hite, R.J., (1960), Stratigraphy of the saline fades of the Paradox Member of the Hermosa Formation of southeastern Utah and southwestern Colorado. *Geology of the Paradox basin fold and fault belt: Four Corners Geological Society Field Conference, 3rd,* p. 86-89.

Hite, R.J., (1985), The sulfate problem in marine evaporites. *Sixth Symposiumon Salt: The Salt Institute*, v. 1, p. 217-230.

Raup, O. B., & Hite, R. J. (1992), Lithology of evaporite cycles and cycle boundaries in the upper part of the Paradox Formation of the Hermosa Group of Pennsylvanian age in the Paradox Basin, Utah and Colorado. *US Geological Survey Bulletin 2000-B.*

Holt, N. M., J. Garcia-Veigas, T. K. Lowenstein, P. S. Giles, and S. Williams-Stroud (2014), The major-ion composition of Carboniferous seawater, *Geochim. Cosmochim. Acta*, *134*, 317–334.

Jaworska, J. (2012), Crystallization, Alternation and Recrystallization of Sulphates. *Advances in Crystallization Process*, 465-490.

Lynch, G., and P. S. Giles (1995), The Ainslie Detachment: a regional flat-lying extensional fault in the Carboniferous evaporitic Maritimes Basin of Nova Scotia., *Can. J. Earth Sci.*, *33*, 169–181.

Pe-Piper, G., D. J. W. Piper, and S. B. Clerk (1991), Persistent mafic igneous activity in an A-type granite pluton, Cobequid Highlands, Nova Scotia, *Can. J. Earth Sci. = Rev. Can. des Sci. la Terre*, *28*(7), 1058–1072.

Petrychenko O., Peryt T. M. and Roulston B. (2002), Seawater composition during deposition of Visean evaporites in the Moncton Subbasin of New Brunswick as inferred from the fluid inclusion study of halite. *Can. J. Earth Sci*. 39, 157–167.

Quinlan, G. M., and C. Beaumont (1984), Appalachian thrusting, lithospheric flexure, and the Paleozoic stratigraphy of the Eastern Interior of North America, *Can. J. Earth Sci.*, *21*(9), 973–996.

Schenk, P. E., R. Matsumoto, and P. H. Bitter (1994), Loch Macumber (early Carboniferous) of Atlantic Canada, *J. Paleolimnol.*, *11*(2), 151–172.

Stewart, F.H., (1963), Marine evaporites. *Fleischer, M., ed., Data of geochemistry* (6th ed.): U.S. Geological Survey Professional Paper 440-Y, 52 p.

Timofeeff, M. N., T. K. Lowenstein, S. T. Brennan, R. V. Demicco, H. Zimmermann, J. Horita, and L. E. Von Borstel (2001), Evaluating seawater chemistry from fluid inclusions in halite: Examples from modern marine and nonmarine environments, *Geochim. Cosmochim. Acta*, *65*(14), 2293–2300.

Waldron, J. W. F., D. J. W. Piper, and G. Pe-Piper (1989), Deformation of the Cape Chignecto Pluton, Cobequid Highlands, Nova Scotia: thrusting at the Meguma-Avalon boundary, *Atl. Geol.*, *25*, 51–62.

Waldron, J. W. F., M. C. Rygel, M. R. Gibling, and J. H. Calder (2013), Evaporite tectonics and the late Paleozoic stratigraphic development of the Cumberland basin, Appalachians of Atlantic Canada, *Geol. Soc. Am. Bull.*, *125*(5-6), 945–960.

Warren, J. K. (1989), Evaporite Sedimentology: Importance in Hydrocarbon Accumulation. *Prentice-Hall, Inc.*, 38-163.

Williams-Stroud S. (1994), The evolution of an inland sea of marine origin to a non-marine saline lake: the Pennsylvanian Paradox Salt. *SEPM Spec.* Publ. 50, 293–306.

8.0 Appendices

Appendix A - Core Description

Depth (ft)	Core #, Box #	Lithology	Structures	Notes
2811.2-2815.8	2, 9	Halite, clear and dark	Dipping bands, some folding and deformation	Transition from dark to clear and back, broken up
2815.8-2820.5	2,10	No Change	Slightly more deformation	Clear and dark beds intertwined/waving, broken up
2820.5-2825.4	2, 11	No Change	Some vertical bands	No Change
2825.4-2827	2, 12	No Change	No Change	No Change
2830-2835	3, 1	Halite, clear and dark, some silty intervals, Clear dominates	Distinct halite banding, dipping ~60°	Solid, not broken up, banding random
2835-2840	3, 2	No Change	No Change	No Change
2840-2845	3, 3	Dark halite dominates, pink halite or sylvite potential	No Change	No Change
2845-2850	3, 4	No Change	No Change	No Change
2850-2855	3, 5	Dominantly dark halite, some clear halite and mudstone beds	Relatively massive, few preserved mudstone beds	Mix of halite in places creating grey halite
2855-2860.8	3, 6	No Change	No Change, but more preserved beds	No Change
2860.8-2866.2	3, 7	Dark Halite, Mudstone beds, Sylvite	Grades from preserved mudstone beds to brecciated	Brecciation dominant in second half, broken into pieces
2866.2-2871.6	3, 8	Mudstone, Sylvite	Brecciated material	No Change
2871.6-2877.5	3, 9	No Change	No Change	Some sylvite dominated portions
2877.5-2883.6	3, 10	Brecciated back to creamy halite	Seems to show preserved beds in brecciated section	Brecciated area is solid, not broken up, halite broken up
2883.6-2890	3, 11	Clear and Dark halite, preserved mudstone	Banding and bedding both preserved, folding	Mudstone beds pitted, banding is distinct and also gradual
2890-2894.5	4, 1	No Change	Banding dominates and is more regular	Bands are dominant feature
2894.5-2907.7	4, 2-4	No Change	No Change	No Change
2907.7-2916.8	4, 5-6	Dark halite with some pink halite and sylvite grading to brecciated sections	Few preserved mudstone beds going to brecciated material	Brecciated material held together but goes to brittle material
2916.8-2925.7	4, 7-8	Mudstone and Sylvite	Mudstone with sylvite filling gaps	Sylvite showing flow around mudstone clasts
2925.7-2935.5	4, 9-10	No Change	No Change	More broken up
2935.5-2944.9	5, 1-2	No Change	No Change	No Change
2944.9-2949.4	5, 3	More sylvite rich	No Change	No Change

2949.4-2958.3	5, 4-5	Mudstone, Sylvite, Halite	Few preserved mudstone beds	Small halite interval with mudstone beds in middle
2958.3-2963.3	5, 6	Mudstone, Sylvite	Brecciated heavily	Broken up
2963.3-2982	5, 7-10	No Change	No Change	Some portions more held together
2982-2987	5, 11	Mudstone, Sylvite, Halite	Brecciated heavily with small proportion of halite	Broken up
2987-2992	5, 12	Mudstone, Sylvite	Brecciated heavily	Sylvite-rich, held together
2992-2998	5, 13-14	No Change	No Change	More broken up
2998-3014.4	6, 1-4	No Change	No Change	Mix of broken and solid
3014.5-3018.9	6, 5	No Change	No Change	Solid
3018.9-3023.5	6, 6	Mudstone, Sylvite, Halite	No Change	Small halite chunks in broken up core
3023.5-3028.3	6, 7	Grading back to clear and dark halite, some sylvite	Sylvite intermixed with halite, looks to be randomly distributed	Broken up
3028.3-3032.9	6, 8	Less sylvite	Still lacking obvious structures	Becomes solid again
3032.9-3037.5	6, 9	Mudstone, Sylvite, Halite	Brecciated material, some preserved mudstone beds	First half brecciated, second half creamy halite with mudstone beds
3037.5-3042.2	6, 10	No Change	No Change	Brecciated appearance but halite dominated with preserved mudstone beds
3042.2-3046.7	6, 11	Halite, Mudstone	Thin banding, preserved mudstone beds	Portion of core broken and bagged
3046.7-3051.2	6, 12	No Change	No Change	Core more solid
3051.2-3056	6, 13	Halite, Mudstone, Sylvite	Goes from thinly banded halite to brecciated	
3056-3064.5	7, 1-2	Mudstone, Sylvite	Heavily brecciated	Held together
3064.5-3070.4	7, 3	No Change	No Change	No Change
3070.4-3075	7, 4	Halite, Mudstone	Clear to creamy halite with thin preserved mudstone beds dipping ~60°	Hard to determine true halite colour due to external staining
3075-3079.7	7, 5	Same with some pink halite and sylvite	Same with beds ~40° and brecciation at end	Pink halite with bedding, sylvite with brecciation
3079.7-3084	7, 6	Clear, Dark and Pink Halite, Mudstone	Mix of halite banding with preserved bedding	Preserved beds often break up the halite banding
3084-3088.7	7, 7	No Change	Less preserved banding and bedding, becomes brecciated	
3088.7-3092.2	7, 8	Mudstone, sylvite	Heavily brecciated	Solid
3092.2-3098	7, 9	No Change	No Change	No Change

3098-3102.3	7, 10	Some Halite present	Massive halite near end of box	No Change
3102.3-3107	7, 11	Mudstone, Sylvite	Brecciated to heavily brecciated	No Change
3107-3111.6	7, 12	No Change	More mudstone dominated than before, more brittle	Broken up
3111.6-3116.5	7, 13	Clear and Dark halite	Some possible banding	Broken up so structures not evident
3116.5-3121.2	8, 1	Halite, mudstone	Massive dark halite with few preserved mudstone beds	
3121.2-3144.3	8, 2-6	Mudstone, Sylvite, Halite	Brecciated with occasional chunks of broken up halite	Mix of solid and brittle material
3144.3-3149	8, 7	Mudstone, Sylvite, Clear and Dark halite	Have bands of sylvite and mudstone changing into clear and dark halite bands with mudstone beds	Gradual change from brecciated to non-brecciated, well preserved banding
3149-3153.3	8, 8	Halite, Mudstone	Clear and dark halite banding, preserved mudstone beds	Dipping ~30-50°
3153.3-3176	8, 9-13	Some pink halite	Much of the same until box 13 which is mudstone dominated with some sylvite cross cutting beds	Well preserved, dipping but little deformation
3176-3189.7	9, 1-3	Mudstone, Sylvite	Heavily brecciated	Solid
3189.7-3194.3	9, 4	No Change	No Change	No Change
3194.3-3199	9, 5	Slight halite component	Brecciated with massive halite sections	No Change
3199-3203.5	9, 6	No Change	Some deformed, but intact mudstone beds	Some obviously recrystallized halite
3203.5-3212.7	9, 7-8	Halite, Mudstone	Very well defined and preserved mudstone beds	Some halite looks to be recrystallized, others not
3212.7-3236	9, 9-14	No Change	Mudstone beds preserved, dominantly clear halite, little banding	Some pitting and some red staining on exterior
3236-3240.9	10, 1	No Change	Darker halite dominates with same preserved mudstone beds, but are less continuous	Seems to be larger mudstone component in halite
3240.9-3245	10, 2	No Change	Mix of clear and dark halite becoming brecciated	Same red staining seen around mudstone beds
3245-3249	10, 3	Mudstone, Sylvite	Heavily brecciated	Broken up
3249-3252.6	10, 4	No Change	No Change	bagged as broken into fine grained piles
3252.6-3257.3	10, 5	Halite, Mudstone	Drastic switch to well preserved linear mudstone beds in dominantly clear halite matrix with	Pitting of mudstone bids and bed dip ~40-60°

			some dark halite bands present	
3257.3-3261.8	10, 6	No Change	No Change	No Change
3261.8-3265.8	10, 7	No Change	Halite bands dominate over preserved beds	No Change, bands mirror dip
3265.8-3270.5	10, 8	No Change	No Change	No Change
3270.5-3275.1	10, 9	No Change	Less obvious structures, looks more massive	Exterior stained, obscuring any obvious banding
3175.1-3280	10, 10	No Change	Some mudstone beds preserved but hard to determine	No Change
3280-3284.6	10, 11	No Change	No Change but more dark halite	No Change, some red staining on exterior
3284.6-3289.2	10, 12	No Change	No Change	No Change
3289.2-3294	10, 13	Mudstone, Sylvite	Heavily brecciated	Silty, bagged material
3294-3298.6	11, 1	Mudstone, Sylvite, Halite	Heavily brecciated moving to blocky halite chunks	Bagged moving to small chunks of halite
3298.6-3302.3	11, 2	Mudstone, Halite	Mix of clear and dark halite, few preserved beds	Mudstone pitting, red staining
3302.3-3307.7	11, 3	No Change	Well preserved beds, some thin bands but mainly clear halite dominated	No Change, beds dip ~20-50°
3307.7-3312.3	11, 4	No Change	No Change	No Change
3312.3-3316.6	11, 5	No Change	Larger mudstone component, with some areas breaking into piles of silt	No Change
3316.6-3321.3	11, 6	No Change	Preserved mudstone beds and thin bands	No Change, becomes brecciated at end
3321.3-3326.1	11, 7	Mudstone, Sylvite	Brecciated	
3326.1-3330	11, 8	Halite, Mudstone, Sylvite	Mainly massive halite with few mudstone beds and small proportion of brecciated material	
3330-3347	11, 9-12	Mudstone, Sylvite, Halite	Dominantly brecciated, some mudstone portions with sylvite and other areas show preserved halite with mudstone beds that is more broken up	Some sections bagged, some still fully intact, mudstone beds show pitting
3347-3355	11, 13-14	No Change	Generally massive mudstone/sylvite mixture	Solid
3355-3363.5	12, 1-2	Mudstone, Sylvite	Brecciated, sylvite filling fractures in mudstone	Some bagged, some in tact
3363.5-3368	12, 3	Mudstone, Sylvite, Halite	Dominantly massive grey halite with a component of	

			mudstone and some brecciation	
3368-3397.4	12, 4-10	Mudstone, Sylvite	Heavily brecciated	Bagged to small blocks of mudstone with sylvite
3397.4-3402	12, 11	Halite, Mudstone	Massive clear halite with some indications of preserved mudstone beds	Some red staining, some pitting on mudstone
3402-3406.5	12, 12	No Change	Slightly more dark halite, higher mudstone component	No Change
3406.5-3415	12, 13-14	No Change	Preserved mudstone beds evident, clear and dark halite bands	Mudstone beds break/define bands often
3415-3424.9	13, 1-2	Mudstone, Sylvite	Dominantly mudstone with sylvite filling fractures in matrix	Some portions breaking down to silt piles
3424.9-3428.9	13, 3	Halite, Mudstone	Dominantly creamy halite with some mudstone component, not beds though	
3428.9-3433.4	13, 4	Mudstone, Sylvite, halite	Brecciated material with small areas of halite	Broken up
3433.4-3438.2	13, 5	No Change	Brecciated material that shows some mudstone and sylvite banding, clasts seem to have an orientation which follows banding	Solid
3438.2-3442.8	13, 6	No Change	Some preserved mudstone beds, some areas of pure sylvite, less deformation	No Change
3442.8-3451.5	13, 7-8	Mudstone, Sylvite	Heavily brecciated, sylvite fills cracks	Mostly piles of mud and silt with sylvite chips present in gaps
3451.5-3456.1	13, 9	Halite, Mudstone, Sylvite	First half is massive dark halite with preserved mudstone bed, but goes back to brecciated material	
3456.1-3460.7	13, 10	No Change	Brecciated material	Small proportion of halite
3460.7-3465.1	13, 11	Halite, Mudstone, Sylvite	Dominant mixed colour halite with few preserved bed and small proportion of sylvite at beginning	Brecciation still present for first ~20 cm of box
3465.1-1-3475	13, 12-13	Halite, Mudstone	Dominantly clear massive halite with preserved linear mudstone beds, some halite banding	Mudstone beds dip ~60-70°
3475-3483.9	14, 1-2	Halite, Mudstone	Mix of clear and dark halite bands on a fine	No Change

			scale to dominantly dark halite, with mudstone beds throughout	
3483.9-3520.8	14, 3-10	Mudstone, Sylvite	Heavily brecciated, sylvite filling fractures	Solid generally
3520.8-3535	14, 11-13	Halite, Mudstone	Clear and dark banded halite, preserved mudstone beds	Some obvious recrystallization and staining near mudstone beds (staining looks an orangey red colour)
3535-3544.2	15, 1-2	Halite, Mudstone	Seem to have some brecciated halite at start that moves into clear and dark halite (some banding) with some pink halite and mudstone beds	Some halite recrystallized, most of mudstone beds breaking down
3544.2-3553.8	15, 3-4	Halite, Mudstone	Dominantly massive dark halite, some clear recrystallized clear halite portions	Mudstone present within halite, but not as discrete beds
3553.8-3558.4	15, 5	No Change	Dominantly massive dark halite with some preserved mudstone beds	Beds dip ~40°
3558.4-3562.5	15, 6	Mudstone, Halite, Sylvite	Recrystallized halite becomes brecciated material	Recrystallized halite is mainly dark with few clear circular inclusions
3562.5-3566.8	15, 7	Mudstone, Sylvite	Heavily brecciated	Large proportion of sylvite – red staining of box
3566.8-3575.9	15, 8-9	Halite, Mudstone	Abundant preserved mudstone beds, some clear and dark halite banding and mixing	Beds dip at ~50°
3575.9-3580.5	15, 10	No Change	Similar but slightly higher mudstone component	Mudstone component making halite more brittle
3580.5-3585.3	15, 11	No Change	Dark halite dominated, high mudstone component, some mudstone beds	Mudstone beds dip shallowly at ~20° and second half of box is broken up
3585.3-3594.6	15, 12-13	No Change	Clear and dark halite, mudstone beds preserved, also have large mudstone component	Mudstone causes halite to be more broken up, more brittle/crumbly
3594.6-3609	16, 1-3	Halite, Mudstone, Sylvite	Starts as dark mudstone rich halite, grades into bagged brecciated material and back to dark mudstone rich halite,	Abundant change over small interval

			ending in a clearer halite section	
3609-3613.5	16, 4	Mudstone, halite	Clear halite dominated with preserved mudstone beds	Some red staining and pitting on mudstone, beds dip from ~20-45°
3613.5-3618.6	16, 5	No Change	Dark halite dominated with small clear halite bands and mudstone beds	No Change
3618.5-3654.2	16, 6-13	Halite, Mudstone, Sylvite	Slow gradual change from banded halite with mudstone beds to red-stained, brittle brecciated material dominated by mudstone	Goes from halite, to brecciated material, back to halite and then becomes fully brecciated, doesn't occur immediately
3654.2-3714.2	17, 1-13	Mudstone, Sylvite	Heavily brecciated, mudstone dominated, sylvite present in fractures, flowing around mudstone clasts	Generally quite solid, some silt piles where is almost all mudstone
3714.2-3757.1	18, 1-9	No Change	No Change	More broken up and degraded
3757.1-3766.8	18, 10-11	Mudstone, Sylvite, Halite	Less deformed, some banding and bedding preserved, still signs of recrystallization	Lower mud content, less broken up
3766.8-3771.6	18, 12	No Change	All bagged, heavily brecciated with some small pieces of halite	Basically piles of silt
3771.6-3798.9	19, 1-6	No Change	Almost all bagged, some halite chunks present and not bagged	Halite is stained and looks obviously altered
3798.9-3803.6	19, 7	Halite, Mudstone	External surface heavily stained but seems to be some banding and few preserved beds	Still in rough shape but not brecciated, some red and orange staining
3803.6-3817.2	19, 8-10	No Change	Less banding, less bedding, obvious recrystallization	Red and orange staining more prevalent
3817.2-3830	19, 11-13	No Change	Increasing mud content reducing much of sample to silt piles	Same staining seen where samples intact
3830-3833	20, 1	No Change	Features (likely preserved mudstone) that look almost stylolitic, generally cream coloured halite	Staining still prevalent and some crumbling from high mud content
3833-3865.7	20, 2-8	No Change	High mud content causing some crumbling, variable clear and dark halite bands and preserved	Exterior stained but core generally in good shape, some mixing of clear and dark halite from recrystallization,

			beds despite some obvious recrystallization	banding boundaries blurred
3865.7-3875.1	20, 9-10	Mudstone, very small portion of sylvite	Bagged piles of mud and silt	Very little sample, only few bags present
3875.1-3889	20, 11-14	No Change	No Change	No Change
3889-4009.8	21-23, all	No Change	No Change	No Change

Appendix B - Sample Description

From top of hole down
Starting at closest to surface and going to greatest depth
* indicate further study considered

Sample: 42 *
Area in core: Core 2, Box 11, ~2822 ft depth
Size: 13.5cm x 8.7cm
Texture: relatively coarse-grained, well defined and formed crystals that are interlocking with clean fresh faces (grains average from 3-5mm), light and dark blend together over 2cm window
Structures: some form of bedding/banding between creamy-white/clear halite and darker grey halite (bed dips at ~60 degrees). The banding is deformed and wavers, likely due to the salt expulsion
Composition: creamy-white/clear halite and darker grey halite
Other: geochemical data already present from this area

Sample: 41 *
Area in core: Core 3, Box 2, ~2841 ft depth
Size: 6.4cm x 8.8cm
Texture: relatively coarse grained (clear/milky halite grains 3-6mm and dark grey halite grains 1-4mm), well defined and formed crystals that are interlocking with clean fresh faces. Dark halite and clear halite blend together at a gradual boundary, not abrupt (over 1cm window)
Structures: bedding/banding seen between the clear/cream halite and dark halite with bed dipping between 20-70 degrees (bed doesn't waver but is curved) with average dip of 40 degrees
Composition: creamy/clear halite and dark grey halite
Other: seems that some grains are completely clear and some are more creamy coloured in sample. Geochemical data not already present for this area

Sample: 40 *
Area in core: Core 3, Box 8, ~2872 ft depth
Size: 11cm x 7.6cm
Texture: brecciated samples with pinky/red matrix (carnallite or sylvite) with finer grains that are very interlocked, hard to see defined grains even with hand lens (~1mm to less) but some clean crystal surfaces can be seen. The rest of the sample is composed of blocky fragments, ranging from 0.2cm-5cm that show a varying composition – some being a darker grey green

colour, which are fine grained, smooth, and have a silky sheen to them (almost look platy), whereas others are a lighter brown green colour and are coarser grain, feel sandy or silty to the touch and lack a sheen. These blocky chunks have grains of carnallite or sylvite caught up in them (mainly in the grittier sandier blocks)
Structures: no obvious structures, doesn't show a preferred orientation or any banding
Composition: carnallite or sylvite matrix with blocks of mudstone to poorly consolidated sandy/siltstone
Other: no previous geochemical data present

Sample: 39 *
Area in core: Core 3, Box 11, ~2889 ft depth
Size: 10.9cm x 8.8cm
Texture: relatively coarse-grained creamy/clear halite (3-6mm) and dark halite (2-5mm) banded/bedded with a mudstone lamination on either side of the darker halite bed. The darker halite blends into the clear halite despite the mudstone bed on ~2cm spread. Mudstone bed is thin (0.2-1cm), but only a remnant. All that is left is small pits with some muddy material remaining. Pits range from 0.2-1cm across and are 0.2cm-1.6cm long. In other words they are not completely connected and are just a spotted band on either side of the dark grey halite bed
Structures: bedding in sample is relatively consistent, with little wavering, possibly good for sampling as still have the mudstone bed preserved to a degree. Bed dips at ~50-60 degrees
Composition: creamy/clear halite, dark grey halite, mudstone pockets
Other: geochemical data present for this sample

Sample: 36
Area in core: Core 4, Box 3, ~2900 ft depth
Size: 10.4cm x 8.9cm
Texture: relatively coarse-grained creamy/clear halite (2-7mm) and dark grey halite (1-6mm). On fresh surface can clearly see abundant interlocking grains that are easily distinguishable in clear halite, but less distinguishable in dark grey halite. Not a well-defined bed/band, more of a dark grey halite line with gradual fading towards creamy halite outwards in either direction over a ~2-3cm scale
Structures: band/bed not defined but as mentioned above seems to be a darker grey halite zone that has leached outward or been altered outward from dark grey halite line – rough dip of ~40-60 degrees on bed
Composition: creamy/clear halite and dark grey halite
Other: no geochemical data currently present

Sample: 37 *
Area in core: Core 4, Box 4, ~2906 ft depth
Size: 12cm x 8.9cm
Texture: relatively coarse-grained with almost all dark grey halite with patches of clear/creamy halite present within. Potential banding, but looks deformed and on smaller scale, cm thick bands that pinch and swell and blend into a medium grey colour, not continuous. Similar to previous have more defined grains in clear halite and more interlocked grains in grey halite

Structures: rough banding of dark, clear, dark, clear, dark, clear across sample, but not visible throughout entirety of section – from what can be discerned, bands waver between a dip of 50 and 70 degrees
Composition: mix of clear halite and dark halite (mostly dark grey) which also creates a lighter grey halite appearance (maybe light grey grains or maybe just the mixture creates the appearance
Other: no geochemical data

Sample: 38 *
Area in core: Core 4, Box 7, 2920 ft. depth
Size: 6.3cm x 8.8cm
Texture: relatively coarse-grained carnallite or sylvite (1-5mm) with grains that are distinguished and well defined. Some areas where grains are packed very closely together and others where they stand out more. Potential preferred orientation of the grains, look slightly elongated looking down the sample (downhole), aka elongated across hole. Also have a mudstone component defined by relatively large blocks with sharp contacts and have abundant carnallite/sylvite within block. Mudstone portions are a pinky/red/brown colour and are gritty, well held together – basically muddy matrix with carnallite or sylvite grains supported within
Structures: no structure other than potentially elongated grains across hole
Composition: carnallite or sylvite with mudstone
Other: no geochemical data

Sample: 35 *
Area in core: Core 5, Box 10, ~2980 ft depth
Size: 8.4cm x 5.2cm
Texture: coarse-grained dark grey dominated halite sample with some patches of clear halite (2-8mm size grains), can see defined faces on both clear and grey halite, seems as though there are distinct patches, clear halite doesn't blend into dark grey halite, instead is butted up against, but looks separate, little mudstone portion running through sample
Structures: no obvious structures, relatively massive
Composition: clear halite, grey halite, very small mudstone component
Other: geochemical data for rough window present

Sample: 34 *
Area in core: Core 5, Box 13, ~2994 ft depth
Size: 9.6cm x 6.4cm
Texture: relatively coarse-grained sample that has grains ranging from 1-6mm. very interesting as have overall dark grey halite but has slight mudstone component, with little bit of clear halite at edges of sample and abundance of pinky/orange grains throughout centre. Looks to have both carnallite and sylvite present, which are intermingling with the dark grey halite. On outside of sample (slightly polished outside of core) there are abundant pits from where crystals of carnallite or sylvite have weathered out or been dissolved. Seem to be in a line, potential bedform?

Structures: possible bedform of intermixed carnallite, sylvite with dark grey halite in between dark grey halite on either side. Defined by pits from weathering, only real way to distinguish bedform clearly, which dips at ~45 degrees
Composition: dark grey halite, clear halite, portions of mudstone in matrix and carnallite and sylvite
Other: geochemical data not present, seems as though carnallite and sylvite may have intruded later through fracture zone or something as seems they fill spaces

Sample: 32 *
Area in core: Core 7, Box 4, ~3070 ft depth
Size: 6.3cm x 8.8cm
Texture: coarse-grained mainly clear halite dominated sample, with small sections of very dark grey halite, also some pinky/orange in one corner, potentially some alteration or differing composition present within that is emitting colour. Grains roughly 0.2-0.8cm in size and can see many clean fresh faces, as per usual, clear looks more separated grains, while grey looks like more interlocked grains, less distinguished
Structures: very interesting structures, in bottom corner dark grey halite band, then have clear halite band, then very thin (0.3cm) band of dark grey halite again followed by a pinky/orange halite above band. Also have a thin (0.3cm) dark grey band cutting through the clear halite section and connecting the two dark grey halite beds, beds dip at just under 50 degrees (~48)
Composition: dark grey halite, clear halite, pink/orange halite
Other: no geochemical data present

Sample: 33
Area in core: Core 7, Box 10, ~3104 ft depth
Size: 4.3cm x 8.9cm
Texture: range of grain size – from too fine to tell up to 6 or 7mm. mainly a pink/orange halite with colour ranging from pink to orange across sample. Also have blocks of mudstone that is a green/brown/dull grey colour that has carnallite or sylvite grains present within. The mudstone is gritty and poorly held together, can scratch and pull apart with fingernail, is crumbly. Carnallite/sylvite grains within are circular and nicely formed, some pitting from grains weathering out. Unsure whether matrix is carnallite/sylvite or just a pink/orange halite
Structures: no obvious structures present
Composition: mudstone with carnallite/sylvite and either carnallite/sylvite or pink/orange halite
Other: geochem data at 3110 but not at 3104

Sample: 29 *
Area in core: Core 8, Box 1, ~3120 ft depth
Size: 5.4cm x 8.8cm
Texture: relatively coarse-grained (1-4mm) dark grey dominated halite. Most uniform sample to date, almost all dark halite, some small patches of clear halite but <5% likely
Structures: no obvious structures, looks relatively massive
Composition: dark grey halite, small portion of clear halite
Other: geochemical data present

Sample: 28
Area in core: Core 8, Box 5, ~3139 ft depth
Size: 7.2cm x 8.8cm
Texture: interesting texture, generally coarse-grained (2-5mm) pink/orange halite or carnallite/sylvite matrix that has a mudstone component in blocks similar to before, except these are finer grained blocks, darker and better consolidated, less crumbly. Still have carnallite/sylvite grains trapped within. Blocks are a dark grey green colour
Structures: no obvious structures other than potential for elongated grains across drill hole as seen before in similarly altered sample
Composition: orange/pink halite or carnallite/sylvite and mudstone with carnallite/sylvite grains within
Other: no geochemical data

Sample: 27 *
Area in core: Core 8, Box 8, ~3153 ft depth
Size: 13.0cm x 8.2cm
Texture: fresh face obscures bedding but on outer surface can see very thin fine scale cyclic bedding – beds of clear and grey halite, little then lenses of mud between many of the bed planes
Structures: beds at 50 degrees
Composition: clear, grey halite and mudstone
Other: no geochem data

Sample: 26 *
Area in core: Core 8, Box 9, ~3158 ft depth
Size: 11.0cm x 7.7 cm
Texture: very nicely bedded clear, grey halite section with some cream interspersed at bedding planes. Coarse grained (3-7mm) with nice fresh face
Structures: beds dip at 45-60 degrees and range from cm to several cm thick
Composition: clear, grey halite and cream halite
Other: no geochem data

Sample: 25 *
Area in core: Core 8, Box 11, ~3164 ft depth
Size: 8.4cm x 7.9cm
Texture: pretty coarse (2-7mm), half grey halite and half clear halite, contact is blurred so can't tell bedding plane but only slightly altered, some mudstone component in grey halite
Structures: bedding but can't measure dip as is gradual contact
Composition: clear and grey halite, little mud
Other: no geochem data

Sample: 24 *
Area in core: Core 8, Box 12, ~3167 ft depth

Size: 8.6cm x 8.1cm
Texture: another beautifully bedded sample with clear, cream and grey halite (2-6mm), once again a thin lens of mudstone
Structures: beds at 65-75 degrees roughly, waver a bit, looks intact though, possibly unaltered
Composition: clear, cream, grey halite and mudstone
Other: no geochem data

Sample: 23 *
Area in core: Core 9, Box 9, ~3214 ft depth
Size: 8.7cm x 8.4cm
Texture: coarse grained almost exclusively clear/cream halite (massive)(3-7mm) with one thing laminae of mudstone indicating a preserved bedding plane
Structures: bedding roughly at 50 degrees based off mudstone bed
Composition: clear/cream halite, mudstone
Other: no geochem data

Sample: 22 *
Area in core: Core 10, Box 6, ~3258 ft depth
Size: 13.2cm x 8.7cm
Texture: gorgeous sample of interbedded clear, cream, grey halite with some preserved mudstone beds seen through pitting on the outside of the sample. Grains from 1-6mm
Structures: beds at 50-60 degrees and ranging from 0.5cm to couple cm thick beds
Composition: clear, cream and grey halite with some mudstone
Other: no geochem data

Sample: 21
Area in core: Core 10, Box 10, ~3276 ft depth
Size: 2 chunks – 1st 9.8cm x 4.6cm, 2nd 9.0cm x 3.7cm
Texture: mix of clear and grey halite with no obvious bedding or orientation. Possible contact between the two where it becomes distinguished and separated but unsure due to broken sample. Grains from mm-5mm
Structures: none, possible vertical bed though
Composition: clear and grey halite
Other: no geochem data

Sample: 31
Area in core: Core 11, Box 2, ~3299 ft depth
Size: 7.5cm x 5.7cm
Texture: coarse grained sample with clear halite in centre and orange/pink altered halite on outside. Definite deformation occurred in area and have grains from 2-5mm with average in middle
Structures: no structures, just decreasing deformation into centre, or decreased fluid interaction/staining
Composition: orange/pink halite and clear halite

Other: no geochem data

Sample: 30 *
Area in core: Core 11, Box 7, ~3325 ft depth
Size: 13.5cm x 8.0cm
Texture: mostly dark grey halite with some lighter cream halite and clear halite as well. Grains on the sub mm scale (mud component) up to the 5-6mm scale in some of the coarser grey and cream and clear halite
Structures: no obvious indicators of bedding but looks like a relatively massive homogeneous dark grey halite sample
Composition: grey halite, cream and clear halite, some mud component
Other: no geochem data

Sample: 03 *
Area in core: Core 12, Box 3, ~3367 ft depth
Size: 4 chunks – 1^{st} is 6.4cm x 8.0cm, 2^{nd} is 7.6cm x 8cm, 3^{rd} is 4.5cm x 2.5cm and 4^{th} is 5.0cm x 2.0cm
Texture: definitely altered, see some grain elongation at 35 degrees to hole, have lots of pink halite present along with grey and clear halite. Grains from 1mm-9mm and no obvious bedding. Unsure of alteration
Structures: only thing is the elongation of crystals at ~35 degree angle to hole
Composition: Pink halite and clear and grey halite
Other: no geochem data

Sample: 02
Area in core: Core 12, Box 11, ~3399 ft depth
Size: 7.6cm x 8.8cm
Texture: quite clean, mostly a light grey/brown halite with some darker and clear portions present, lacking bedding, see some pitting on the back of the sample with pink/red/orange staining around. Grains are coarse and from 1-5mm
Structures: lacking any obvious bedding or other structures
Composition: grey and clear halite, possible remnant mudstone with some maybe carnallite and sylvite that would have weathered out
Other: no geochem data

Sample: 01 *
Area in core: Core 12, Box 13, ~3408 ft depth
Size: 8.9cm x 8.7cm
Texture: beautiful sample that have very nice preserved bedding can see clear halite bed curve around the core sample and on fresh surface have almost complete grey halite with some variations of clear and creamy halite present as well. Grains similar to others 1-5mm with very small mud component
Structures: bedding at 50-60 degrees roughly
Composition: grey halite, clear and cream halite, mudstone

Other: no geochem data

Sample: 20
Area in core: Core 13, Box 2, ~3420 ft depth
Size: 8.5cm x 8.9cm
Texture: heavy brecciated, very fine grained mudstone that is a dark grey/green colour and quite soft, scratchable with nail. Takes up majority of the rock but have some small areas/crystals of carnallite/sylvite in the matrix and have some larger more pervasive carnallite/sylvite veins cross cutting the mudstone
Structures: some veins but they don't appear to have a specific orientation. Possible relict bedding that mudstone has taken on at a dip of 40 degrees roughly
Composition: mudstone, carnallite and sylvite
Other: no geochem data

Sample: 19
Area in core: Core 13, Box 3, ~3425 ft depth
Size: 8cm x 8.6cm
Texture: relatively coarse grained halite with almost vertical banding of clear halite and grey halite with a mudstone component (clear is 1-5mm and grey is sub mm – 3mm)
Structures: banding is vertical but wavers, looks like the addition of mud weakened grey halite and it is deforming and bending, whereas the clear halite is more rigid and holding its shape better
Composition: clear, grey halite and mudstone
Other: no geochem data

Sample: 18 *
Area in core: Core 13, Box 6, ~3441 ft depth
Size: 6.4cm x 6.0cm
Texture: Coarse grained halite with interlocking crystals, some dark grey halite present but most of it is a deep red halite/sylvite. Grain sizes from sub mm to 5mm
Structures: no obvious structures, look like sample has likely been altered
Composition: pink halite, grey halite, sylvite
Other: no geochem data

Sample: 17
Area in core: Core 13, Box 12, ~3468 ft depth
Size: 6.5cm x 8.8cm
Texture: coarse grained grey and orange halite with some obvious alteration and evidence of some brecciation on outer surface, though inner surface looks clean and also shows some clear unaltered halite – grains from 2-6mm
Structures: brecciated portions are seen through grey halite with mud component that looks to have intruded in and also through the presence of the orange/pink halite that seems to have filled cracks/voids
Composition: clear halite, grey halite, orange/pink halite and mudstone

Other: no geochem data

Sample: 11 *
Area in core: Core 14, Box 1, ~3477 ft depth
Size: 5.5cm x 8.4cm
Texture: coarse grained clear and grey halite with some potential staining to pinky halite. Fresh faces on fresh surface
Structures: no obvious bedding structures but mainly composed of clear halite grains that are distinguishable with some darker halite present as well, but in conjunction with clear halite
Composition: clear and grey halite
Other: no geochem data

Sample: 13 *
Area in core: Core 14, Box 9, ~3514 ft depth
Size: 3.7cm x 8.7cm
Texture: almost exclusively dark brown fine grained mudstone with abundant carnallite/sylvite crystals present within the matrix – carnallite/sylvite grains 1-4mm. also see very small clear and grey halite grains at sub mm scale
Structures: none that are apparent
Composition: mudstone with some carnallite/sylvite and minute amounts of clear and grey halite
Other: no geochem data

Sample: 12
Area in core: Core 14, Box 12, ~3529 ft depth
Size: 5.9cm x 8.5cm
Texture: coarse grained clear halite (2-6mm) with finer grained grey halite (1-3 mm with one or two 5mm crystals), is mainly grey halite with smaller portions of clear halite present
Structures: no obvious bedding or other distinguishing structures
Composition: clear and grey halite
Other: no geochem data

Sample: 16 *
Area in core: Core 15, Box 1, ~3536 ft depth
Size: 8.4cm x 8cm
Texture: beautiful sample, with mix of clear and grey halite of coarse grained nature – 1-5mm grain size overall with coarser grains being clear
Structures: very nice bedding present with some thin interbeds on the mm to cm scale. Generally grey in grey and clear in clear but have some distinct clear small grains in grey and vice versa
Composition: clear and grey halite
Other: no geochem data

Sample: 15

Area in core: Core 15, Box 11, ~3582 ft depth
Size: 2 chunks – 1st is 4.5cm x 8.8cm and 2nd is 4.8cm x 8.6cm
Texture: mix of coarse grained clear halite and some finer grained grey halite with mud component, also have some pinkish looking halite that creeps in from edge and looks like some sort of fluid staining
Structures: potential bedding marks but hard to really distinguish or measure, similar orientation to other samples
Composition: clear halite, grey halite with mud and possible altered/stained halite due to fluids
Other: no geochem data

Sample: 14 *
Area in core: Core 16, Box 5, ~3616 ft depth
Size: 7.2cm x 8.9cm but is on angle, goes with rough bedding
Texture: relatively coarse grained, with clear halite (1-5mm) coarser than grey halite (2-3mm), see clear bedding and many fresh faces. Clear halite grains are more distinct then grey halite
Structures: bedding between clear and grey dipping at 45-60 degrees, bed thickness changes
Composition: grey halite, clear halite
Other: no geochem data

Sample: 09 *
Area in core: Core 18, Box 7, ~3746 ft depth
Size: 14.0cm x 8.8cm
Texture: almost all mudstone with some mixed in carnallite/sylvite. On outer portions of sample have break where it becomes pure sylvite? But in centre is almost all mudstone with some small veins of sylvite and little crystals of carnallite in mudstone matrix (grain size of mudstone is too fine to tell and carnallite/sylvite from 3-5mm roughly
Structures: veins cross mudstone at rough dip of 15-30 degrees as they cut across sample
Composition: carnallite, sylvite and mudstone, likely some other halite in small portions that cant be seen easily
Other: no geochem data

Sample: 08 *
Area in core: Core 18, Box 11, ~3763 ft depth
Size: 7.8cm x 8.8cm
Texture: finer grained sample than most of the others, some forms of bedding present. Clear halite has grains from sub mm-4mm and grey halite has grains from sub mm-2mm. have a couple of pits with similar pinkish staining on outside of core
Structures: pits and bedding oriented in the same direction. Dips at ~55-65 degrees
Composition: clear halite, dark grey halite with some possible mudstone and possible carnallite/sylvite that weathered out?
Other: no geochem data

Sample: 07
Area in core: Core 17, Box 10, ~3701 ft depth

Size: 12.6cm x 8.9cm
Texture: heavily brecciated sample with area of fine grained soft mud and area of grey halite mixed with mud component. Mud has dark brown colour, looks like high clay content? And mixed is a lighter green brown colour. Also have carnallite or sylvite patches within the sample filling in fractures or cracks in apparent sheets
Structures: no obvious bedding or other recognizable structure
Composition: grey halite, mudstone, carnallite/sylvite
Other: no geochemical data

Sample: 06
Area in core: Core 17, Box 11, ~3703 ft depth
Size: 11.5cm x 8.8cm
Texture: coarse-grained, see dark halite with potential mudstone component, also see some clear halite and some that is an orangey pink colour. Grains are less than a mm to 7mm
Structures: hard to discern any defined beds, potentially one between dark grey halite with mud and orangey halite at 45-55 degrees, bed pinches and swell. Possible orientation of grains across hole
Composition: clear halite, orange/pink halite, grey halite, mudstone?
Other: no geochem data

Sample: 10 *
Area in core: Core 19, Box 7, ~3800 ft depth
Size: 15.7cm x 8.9cm
Texture: coarse grained (1mm-7mm), mix of clear halite, grey halite with some mudstone present in a small portion, on back side see some pitting from the mudstone with some red/pink staining around the pit, orientation of grains at roughly 45 degrees to the hole
Structures: no obvious bedding but possible thin laminae of grey halite in overall clear halite , with pitting on back following same bedding orientation, dipping at 55-60 degrees, is rough though
Composition: clear halite, grey halite, mudstone, possibly some accessory mineral causing staining? (maybe carnallite or sylvite after being weathered out?)
Other: no geochem data

Sample: 05
Area in core: Core 20, Box 1, ~3830 ft depth
Size: 4 chunks – 1st is 10.4cm x 8.8cm, 2nd is 6.8cm x 8.8cm, 3rd is 6.5cm x 2.7cm and 4th is 4.4cm x 3.2cm
Texture: coarse-grained, possibly banded between clear and grey halite, looks like grains have a preferred orientation roughly across drill hole, grains 1-8mm, clean faces on fresh surface
Structures: possible bedding at 35-40 degrees but is wavy and curved. Also see a contact between a much more mudstone rich section with some interspersed clear and grey halite with occurrences of carnallite or sylvite
Composition: clear halite, grey halite, mudstone, carnallite/sylvite
Other: geochem data present but over a 100ft window – not accurate

Sample: 04
Area in core: Core 20, Box 4, ~3846 ft depth
Size: broken into 4 chunks – 1st is 11.1cm x 8.7cm, 2nd is 12.6cm x 5.3cm, 3rd is 9.4cm x 3.7cm and 4th is 7.0cm x 3.0cm
Texture: coarse grained, mix of clear halite ad darker grey halite. Some clear halite present but looks like it is potentially present as an alteration features. Some good clean crystal faces on fresh surfaces. See some pitting on outer surfaces that should indicate a more fissile mudstone layer but looks to be all halite on the fresh inner surface. Grains generally 2-5 mm. upon closer inspection may be dark halite with some mudstone component
Structures: none able to be seen in this sample
Composition: clear halite, dark grey halite, altered cream halite?, mudstone?
Other: geochemical data from 3806-3908 ft… very broad

Appendix C - XRF Data

XRF data is attached in a separate excel file. Both Run 1 and Run 2 data are represented, though Run 2 was the dominant data set used. Run 1 simply acted to help calculate certain values.

Certain data manipulations were undertaken and are described below.

Firstly, elements not used in this study were discarded from Run 2.

Run 1 calculated relative proportions of elements accurately but did not calculate quantitatively correct values. Run 2 measured more quantitatively accurate values, but found some elements, mainly Br and Mg, under the detection limit. The relative proportions of Cl (for calculating Br) and Ca (for calculating Mg) were calculated between Run 1 and Run 2, giving a conversion factor. This factor was then applied to the Br and Mg values from Run 1 to convert them to more quantitatively accurate values.

The element Na was unable to be measured due to its light molecular weight. However, Run 2 totals all elements measured and provides it as a balance. This balance did not add up to one million, indicating a portion of the sample was not measured. Given that the majority of the samples are halite rich, it is likely that a large proportion of the missing data would have come from Na. Therefore, the balance was subtracted from one million to provide a crude estimate of the Na amount in the samples. It should be noted that this was used strictly as a tool to gather a rough understanding of Na distribution and to ensure it did not vary drastically from Cl. It was not used for any interpretations or analysis.

It should be noted that the XRF does not provide quantitative values that are extremely accurate, but instead provide a helpful first step. Further work using ICP-MS would ideally have been undertaken to receive more quantitatively accurate values if time and money allowed.

Appendix D - Electron Microprobe Data

Electron Microprobe data is attached in a separate excel file.

Certain data manipulations were undertaken and are described below.

Firstly, the oxygen present had to be removed to allow for oxide wt. % to be converted to element wt. %. This was done by dividing the molar mass of the individual element in the formula by the molar mass of the total formula. This calculation created a conversion factor that was then applied to the data.

Ca/CaO = 40/56 = 0.7143
% of CaO microprobe * Concentration factor = Ca %

Next, the data was arranged based on depth and standards were removed, leaving only anhydrite values. Points that were far outside the expected range of data were considered inaccurate or outliers and were removed so as not to greatly skew the average.

This data was then averaged based on the thin section, which also corresponds to a specific depth in the core.

This data was then converted from element wt. % to ppm by multiplying the values by 10,000.

Appendix E - Photo Library

All photos have been compiled into an online photo library which can be viewed via the link:

https://drive.google.com/folderview?id=0B5m8XVFOfpT2ZEFkTVZEWnFjZ28&usp=sharing